Supporting Information Appendix

Long-Read Sequencing Uncovers the Adaptive Topography of a Carnivorous Plant Genome

Tianying Lan, Tanya Renner, Enrique Ibarra-Laclette, Kimberly M. Farr, Tien-Hao Chang, Sergio Alan Cervantes-Pérez, Luis Herrera-Estrella, Chunfang Zheng, David Sankoff, Haibao Tang, Rikky W. Purbojati, Alexander Putra, Daniela I. Drautz-Moses, Stephan C. Schuster, Victor A. Albert

Table of Contents

1. PacBio Sequencing and Assembly of the *Utricularia gibba* genome

1.1. Plant Material

As for our previous short-read genome assembly, *U. gibba* material was sourced from Umécuaro municipality, Michoacán, México, whereafter plants were grown in sterile tissue culture prior to nuclear DNA extraction.

1.2. High Molecular Weight Nuclear DNA Preparation

In order to minimize chloroplast and mitochondrial DNA contamination, high molecular weight DNA was prepared from nuclei of *U. gibba* plants. Nuclear DNA was isolated according to the protocol described by the Mississippi Genome Exploration Laboratory (MGEL; http://www.mgel.msstate.edu/protocols.htm) based on Peterson et al. (1997) (1). The protocol was scaled-down to 10-15 g in order to decrease the amount of tissue required. In addition, isolated nuclei were collected from a 60% Percoll (Invitrogen) density gradient following low-speed centrifugation (4000g for 10 min at 4°C), after which high-quality megabase-sized DNA was isolated.

1.3. PacBio SMRT Sequencing

The quality of the *U. gibba* genomic DNA sample was first assessed by running 150 ng of DNA on a 0.6% pulsed-field agarose gel, stained with SYBR Safe (Invitrogen). Ten µg of DNA were then sheared to a size range of 10-40 kb using a Covaris g-TUBE. The fragment distribution of the sheared sample was validated by pulsed-field gel electrophoresis (Fig. S1A). The sheared DNA was then purified with 0.45X AMPure PB beads (Pacific Biosciences) according to the manufacturer's recommendations. Following the Pacific Biosciences (PacBio®) 20 kb SMRTbell Template Preparation Protocol, library preparation was subsequently performed using 5 µg of the sheared DNA as input. After library preparation, the library was assessed on an Agilent DNA 12000 bioanalyzer chip to determine the optimal cut-off for size selection (Fig. S1B). The libraries were then size-selected on a Sage Science BluePippin instrument using a dye-free 0.75% agarose cassette and 15 kb as the cut-off, followed by reanalysis with the bioanalyzer (Fig. S1C). For *U. gibba*, two libraries were prepared (internal IDs 40a and 40b). Library 40a was sequenced in two SMRTcells on a Pacific Biosciences RSII single-molecule sequencing platform at loading concentrations of 0.15nM and 0.2nM, respectively. Library 40b was sequenced in 8 SMRTcells at a loading concentration of 0.2nM.

A

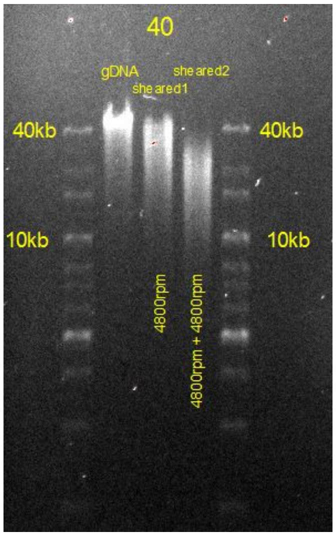

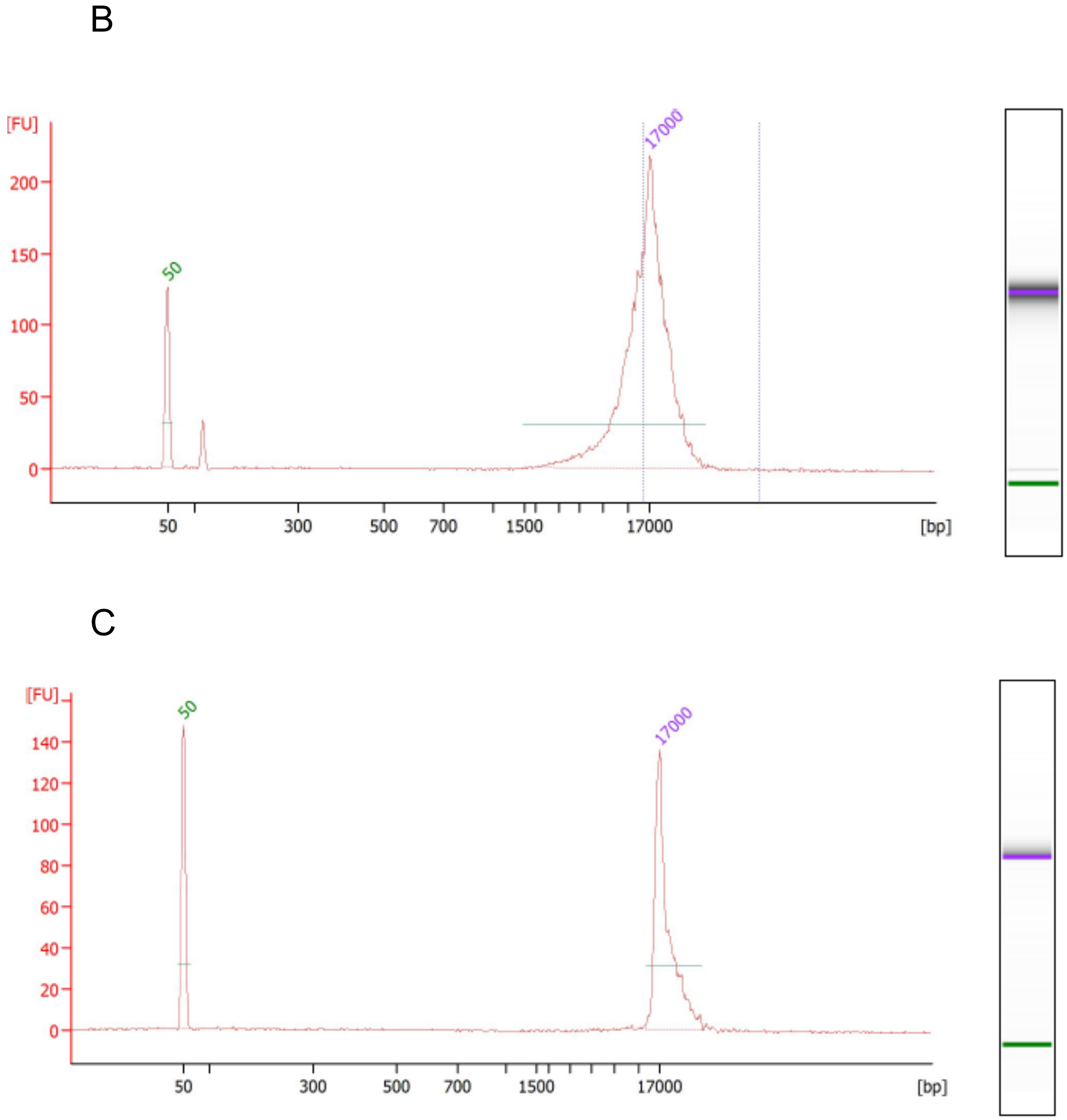

Fig. S1. (A), *U. gibba* gDNA before and after two rounds of shearing (sheared1 and sheared2) using a Covaris g-TUBE. Agilent bioanalyzer profiles for sample 40a, before and after Blue Pippin treatment, are shown in **(B)** and **(C)**, respectively. The spike-in control lies at 50 bp.

1.4. HGAP *De Novo* Genome Assembly

The HGAP3 workflow was used to assemble the raw h5 reads from 10 SMRT cells. The workflow used the software binaries from the SMRT analysis 2.3 package (http://www.pacb.com/products-and-services/analytical-software/smrt-analysis/), and smrtmake (https://github.com/PacificBiosciences/smrtmake) was used as a wrapper for running the HGAP3 workflow. For the initial reads filtering, the "*MinReadScore=0.80, MinSRL=500, MinRL=100*" settings were used. Once the reads were filtered, the workflow attempted to detect overlap between reads. This step was done with the *"-bestn 10 -nCandidates 10 -noSplitSubreads -maxScore -1000 -maxLCPLength 16 -minMatch 14*" parameters. The result of this overlapping step was used to produce a set of corrected reads. Afterward, the corrected reads were used in the assembly process. The HGAP3 parameters used for this step were "*genomeSize = 90000000, xCoverge = 20, defaultFrgMinLen = 500, ovlErrorRate = 0.06, ovlMinLen = 40, merSize = 14*". The genome produced by HGAP3 consists of 581 contigs with N50 of 3,424,836 bp and 101,949,210 total bases (Fig. S2). We used this *de novo* assembly for all downstream analyses. A previous flow cytometry analysis estimated a genome size of 77Mb for *U. gibba*. However, the estimation was carried out using Golden Path *Arabidopsis* genome size (1C = 0.1605 pg or 135 Mb) as an internal standard calibration (2). In fact, *Arabidopsis* lines were proved to exhibit massive genome size variation, ranging from 161 to 184 Mb (3). Consequently, using this *Arabidopsis* genome size range as calibration, the flow cytometry estimated *U. gibba* genome size would be from 92.3 to 105.5 Mb, which is nicely consistent with our current PacBio genome size ~102 Mb.

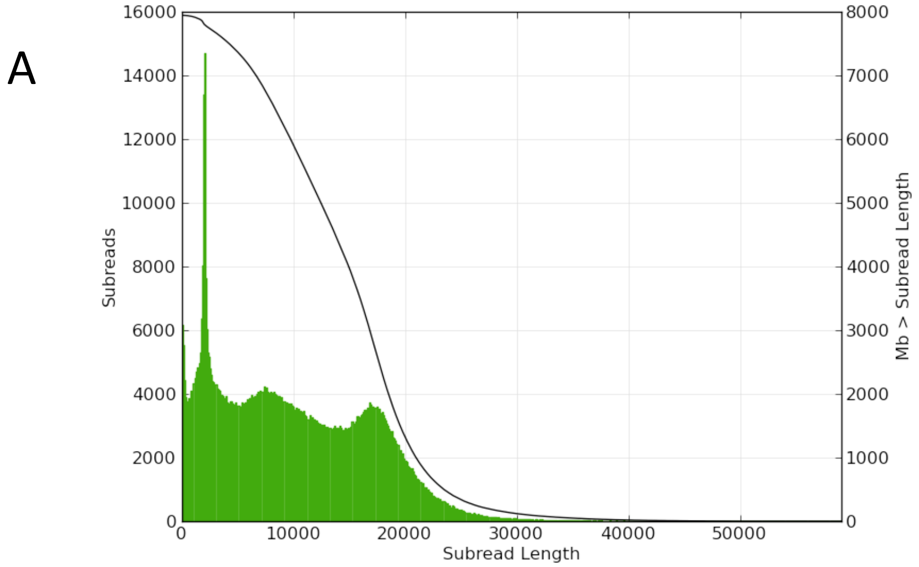

B

	Raw Subreads (Post-Filter Polymerase Reads)	Filtered Subreads	Corrected Reads	Assembly
#Reads	521,937	702,640	155,051	-
#Contigs:	-	-	-	581
Average Len:	15,366	10,385	12,322	175,774.50
Total Bases:	8,020,277,606	7,297,249,484	1,910,594,344	101,949,210.00
Max Len:	59,061	59,061	39,438	8,502,017.00
N50:	21,825	15,244	17,834	3,424,836.00

Fig. S2. Reads and assembly statistics for the *de novo U. gibba* PacBio genome assembly. (A) Raw reads distribution plot. (B) Reads and assembly statistics.

1.5. Testing Genome Assembly Quality Using PacBio and MiSeq Read Data

To test for assembly quality at the nucleotide level, we also polished it using the Quiver workflow (4). The parameters used for this step were *“--forQuiver --seed=1 --minAccuracy=0.75 --minLength=50 --algorithmOptions="useQuality -minMatch 12 -bestn 10 -minPctIdentity 70.0" --hitPolicy=randombest*”. At this step, 72,485 (0.071%) bases were corrected out of 101,810,468 bp total. In addition to the Quiver polishing, a set of Illumina MiSeq data (NCBI BioSample SAMN01940705, from (2)) was also used to provide a measure of assembly quality. A total of 3,120,016,344 base pairs reads (~39x coverage) were used with Pilon (5) to solve any discrepancies between the HGAP3 assembly and the MiSeq data. The settings that were used for this step were “*--fix all, --mindepth 0.1, --mingap 10, --K 47*”. After this step, only 11,053 (0.01%) bases were corrected out of 101,203,230 total, which together with the Quiver statistics verifies the high quality of our PacBio assembly.

1.6. Identification of Contamination and Organellar Contigs

1.6.1. Identification of Environmental Sequence Contamination

Contigs with length < 1 Mb were blasted against the NCBI refseq non-redundant nucleotide database using NCBI blastn (6) v.2.2.30+ with an *E*-value threshold of 1E-5. Contigs with non-plant matches were determined to be environmental sequence contamination. In total, 65 contigs (1,260,662 bp) representing 0.01% of the genome were identified as bacterial contaminants. Among them, 62 contigs (1,171,157 bp) originated from *Methylobacterium*, a common bacterial contaminant of DNA extraction kit reagents (7).

1.6.2. Identification of Plastid and Mitochondrial Genome Contigs

Organelle DNA contigs were identified by: (1) blastn searches against the NCBI refseq non-redundant nucleotide database and, (2) using all available NCBI *U. gibba* organelle DNA from (2) as blastn queries against the new PacBio assembly with an *E*-value threshold of 1E-5. The chloroplast genome was assembled into a single 172,489 bp contig, which gained 20,376 bp compared to the previous 152,113 bp circular assembly (NC_021449.1; (2)). However, further investigation of the linear plastid contig showed that there are two identical terminal regions, while there is only one corresponding region in the previous plastid genome. Therefore, we speculate that the extra sequence in current chloroplast genome is likely misassembled and caused by using a linear *de novo* assembly strategy to assemble a circular genome. Our previous mitochondrial genome assembly constituted ten unique scaffolds/contigs with a combined total length of 222,145 bp (2), whereas the PacBio mitochondrial genome assembled into a single 283,823 bp contig. Due to the dynamic intramolecular recombination of mitochondrial DNA in plant cells, it is common to obtain multiple partially overlapping mitochondrial chromosomes in *de novo* assemblies (8-10).

2. Annotation

2.1. TE annotation and Repeat Masking

Prior to gene prediction, the REPET pipeline v2.2 (11, 12) was used for the *de novo* detection and annotation of transposable elements (TEs). The REPET TE annotation process was carried out in two phases: (i) *de novo* discovery and identification of TE families present in the genome studied, and (ii) the precise, comprehensive annotation of TE copies on contigs or scaffolds. TEs were predicted based on their typical features, and their quality was assessed by the extent to which full ancestral TE reference sequences were recovered andbased on their similarities to high-quality sequences available in public databases (Repbase (13) in this study). TE classes were classified based on Wicker’s classification. (14) The annotation pipeline was performed for both the current PacBio assembly and our previous 454/Illumina/Sanger hybrid assembly (2). The number of annotated TEs, their lengths (range and average), the total bases contained, and the percentages that they represent of total genome space were calculated (Dataset S1). Considering the high recombination rates previously suggested to be linked with

DNA loss in *U. gibba* genomic regions with relaxed selective pressures (2), repeat masking was subsequently performed with RepeatMasker (http://www.repeatmasker.org/) using the library generated by REPET. Option -s was used (slow search; 0-5% more sensitive, 2-3 times slower than default), as was –cutoff. Cutoff score describes the overall quality of the alignments, with higher numbers corresponding to higher similarities for masking repeats with a custom library; a score of 250 was used in this study. This repeat masking strategy was also employed for both the current PacBio assembly and the previous 454/Illumina/Sanger hybrid assembly. Finally, the percentages of genome space assigned to TEs and TE-like regions in both genome assemblies were calculated, and the comparison is illustrated in Dataset S1 and Fig. S3. In summary, a total of 1,121 repetitive sequences were identified in our PacBio assembly, almost 3.5 times more TEs than identified in the published 454/Illumina/Sanger hybrid assembly (2). The percentage assigned to TEs plus TE-like regions in the current assembly is around 59%, which is about 16.5% more than that of the previous assembly. Complete TEs amounted to 8.9% and 2.3%, respectively. These figures can be compared with the 3% reported by Ibarra-Laclette et al. for the latter genome (2). One of the retrotransposon classes, the LARD class (Large Retrotransposon Derivatives), represents around 47% of total TE/TE-derived space identified in the current assembly. Interestingly, this class occupied only about 14.6% of TE/TE-derived space in the published short-read assembly. Increased identification of LARDs in the current assembly results from the capability of long read sequencing to obtain sequences from complex genomic regions with highly repetitive elements and condensed DNA structure (e.g., centromeres and telomeres).

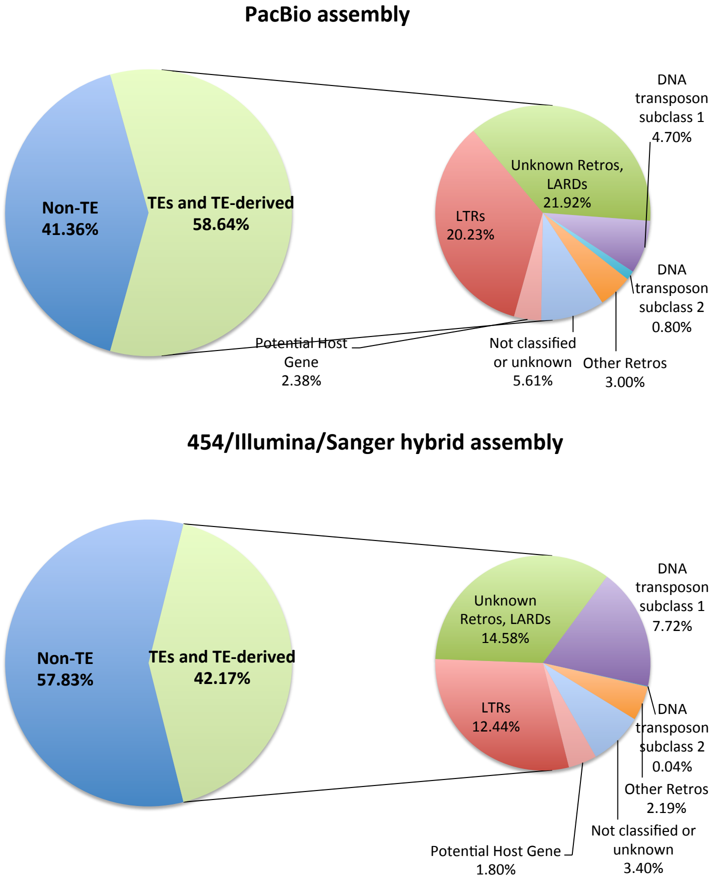

Fig. S3. Comparison of TE composition between the PacBio assembly and the 454/Illumina/Sanger hybrid assembly (2).

2.2. Non-coding RNA (ncRNA) Annotation

rRNA and tRNAs genes were identified using RNAmmer (15) and tRNAScan-SE (16), respectively. Other predicted ncRNA elements, including miRNAs, snRNAs and H/ACA box snoRNAs, were identified by the INFERNAL software (17) using the RFAM database (18, 19) records as models.

2.3. Identification of Protein-coding Genes

Gene models were predicted with an evidence-directed AUGUSTUS predictor (20). AUGUSTUS was trained for *U. gibba* gene parameters using full coding sequences (CDS) derived from gene models predicted for the previous version of *U. gibba* genome (2). This *U. gibba*-specific training set was generated through the Augustus training web interface (21) using only those CDS for which the gene model previously predicted represented "complete CDS", i.e., when proteins derived from the predicted genes represented at least 75% of the length of homologous proteins identified in related asterid species such as *Solanum lycopersicum* and *Mimulus guttatus*. AUGUSTUS was run for genomic PacBio contigs using default parameters, unigenes derived from transcriptome assemblies (2, 22), and those *U. gibba*-specific parameters calculated from the training set. In addition, gene models predicted by AUGUSTUS were complemented using the Maker-P pipeline (23). Inputs for Maker-P included the *de novo* draft genome assembly of *U. gibba*, *U. gibba* transcriptome assemblies (2, 22), a species-specific repeat library predicted using REPET, protein databases containing annotated proteins for *S. lycopersicum* and *M. guttatus* (downloaded from the CoGe OrganismView database; http://genomevolution.org/CoGe/OrganismView.pl), and gene models predicted by AUGUSTUS on the previously published *U. gibba* genome (2).

2.4. Gene Annotation

All unmasked gene models were first blasted against the Viridiplantae Repbase database 21.02 (24) using NCBI tblastx v.2.2.30+ with an *E*-value threshold of 1E-5. Gene models with at least one match were considered to be (e.g., TE) repeat-associated genes and therefore removed from the set. All filtered gene models were then annotated with the highest alignment score matches using tblastx versus the *Arabidopsis* coding sequences database v10.02 with an *E*-value cutoff of 1E-5.

2.5. Identification of Islands of Repeat Elements Surrounding Certain Tandemly Duplicated Gene Clusters

Some tandemly duplicated genes were difficult to predict with prior masking of repeat elements. Therefore, we performed gene model prediction without masking to discover a number of the tandem duplicate cases referred to below (e.g., sections 6.1 and 6.2, below). As part of our RepeatMasker survey (section 2.1), we were able to determine that incomplete recognition of tandem arrays were in some cases due to genes being surrounded by TEs annotated as LARDs (Large Retrotransposon Derivatives (25)), as visible in the browser plots below (Fig. S4) for cysteine protease and KCS gene clusters (sections 6.1 and 6.2, respectively). We hypothesize that such repetitive DNAs (green) might have facilitated the tandem duplications that generated the arrays (blue gene models).

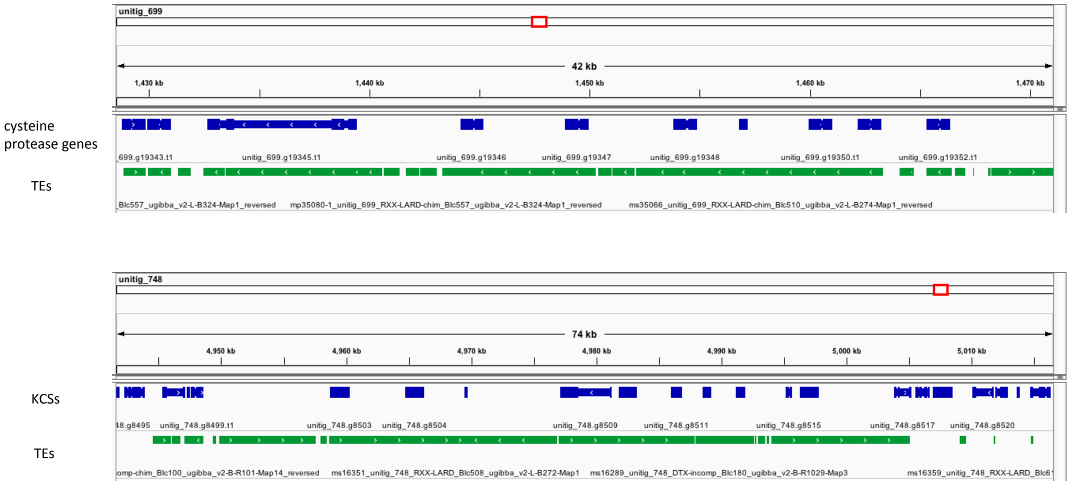

Fig. S4. IGV browser (26) plots showing cysteine protease and *KCS* gene clusters being surrounded by TEs annotated as LARDs.

2.6. Gene Expression Analysis

To investigate genes with trap-enhanced expression in *U. gibba*, 454 RNA-seq raw reads, which were sequenced from *U. gibba* shoot-like structures, traps and inflorescences as separate libraries in our previous study (27), were mapped to the PacBio genome using the subread-featureCounts pipeline (28, 29). The raw reads count table generated by featureCounts then served as input for the edgeR package (30) to calculate $\log_2$ fold change with model-based normalization, a minimum three reads filter, and the dispersion value 0.1 applied. The library size factors calculated by edgeR normalization were ~1 for all three libraries, which indicates that they have a similar library size. Comparisons were performed as traps versus inflorescences, and traps versus shoot-like structures, for which results are summarized in Dataset S2.

3. Identification of Centromeric and Telomeric Sequences

3.1. Identification of Tandem Repeats in the *U. gibba* Genome

We used Tandem Repeats Finder (31) (TRF) to search for tandem repeats in all contigs with alignment parameters 2, 7, and 7 for match, mismatch, and indels, respectively. Additionally, a minimum alignment score of 50 and a maximum period size of 2000 bp (https://tandem.bu.edu/trf/trf.html) were specified. The initial raw TRF output, which included TR arrays with overlapping genomic coordinates, was then processed with a redundancy elimination python script. The redundancy criterion was set to remove the repeat with a larger period size if two repeats shared 90% overlap. However, if the larger repeat had over a two-times greater alignment score, then the smaller repeat was removed. After redundancy elimination, 12,378,680 bp of the genome were annotated as tandem repeats. As shown in Fig. S5A, among repeats, size ranged from 0-600 bp, with the most abundant tandem repeats in the genome being the micro/minisatellite fraction, which has a period size smaller than 50 bp. The other abundant tandem repeats were distributed around 300-360 bp and 520-540 bp. We then performed an all versus all alignment using USEARCH global (32) with settings for ‘global’ alignment and 95% identity threshold. Using a clustering python script, 113 global clusters containing tandem repeats with >90% identity and near identical lengths were produced. Further analysis on tandem repeat clusters was performed for centromeric repeats screening (See section 3.3.2 for details).

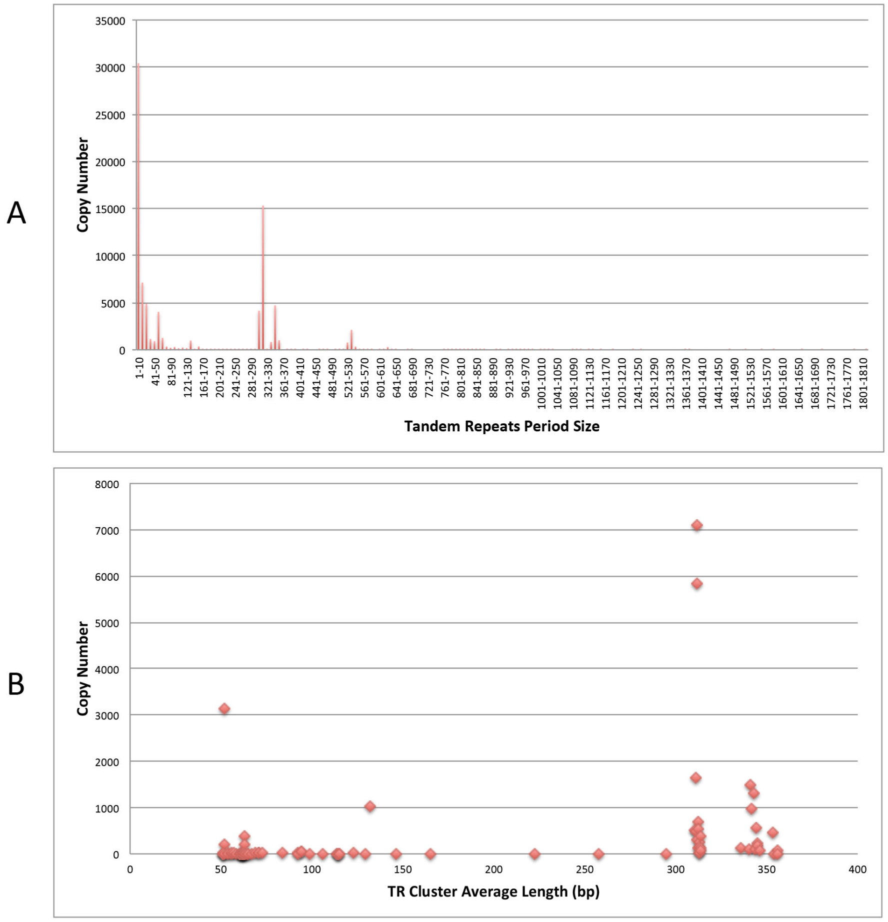

Fig. S5. Distribution plots of tandem repeats and repeat clusters in the *U. gibba* genome. **(A)** The period size and copy number of the tandem repeats identified using TRF. **(B)** The average length and copy number of tandem repeat clusters that had average length < 500 bp.

3.2. Identification of Telomeres

By searching the ends of contigs, high copy numbers of *Arabidopsis*-type telomeric repeats (TTTAGGG) were identified in 24 contigs.s. Two variants - the *Chlamydomonas*-type (33) (TTTTTAGGG) and and a novel type (TTCAGGG, similar to the variants TTCAGG and TTTCAGG known from the close carnivorous plant relative *Genlisea* (34)) - were also found sporadically intermingled with the *Arabidopsis*-type telomeric repeats. Four contigs, for which telomeric repeats were found on both ends, were identified as complete chromosomes. Ten contigs were observed to have internal telomeric repeats, which were identified by searching $(CCCTAAA)_3$ and $(TTTAGGG)_3$ in interstitial regions.

3.3. Identification of Putative Centromeres

The centromere is a complex chromosome component that is responsible for chromosome segregation during meiosis and mitosis. One of the distinctive properties of centromeres is that they are enriched in repetitive elements, including transposable elements (TEs) and tandem repeats (35, 36). Due to the presence and abundance of these identical or near-identical repeats, centromeric regions are a bioinformatic challenge for NGS-based *de novo* genome assembly, and therefore they often remain incomplete and largely uncharacterized even within extensively sequenced and studied genomes (37-39). To resolve this challenge, long reads that exceed TE and tandem array length are needed to obviate misassembly and allow repeats to be unambiguously placed based on unique flanking sequences. PacBio SMRT sequencing, which can generate read lengths up to ~ 20 kb, permitted us to assemble four complete and several near-complete chromosomes, thereby permitting a rare view of the highly repetitive nature of plant centromeres (10).

3.3.1. Identification of Putative Centromeric Regions

For comparing our previous short-read assembly (2) with the new PacBio assembly, a syntenic map was generated using the SynMap tool (40) from the CoGe platform (https://genomevolution.org/CoGe/SynMap.pl). The short-read assembly showed clear gaps within the complete or near-complete chromosomes of the PacBio assembly (Fig. S6). These gaps were the putative repeat-rich centromeric regions that failed to be assembled in the short-read assembly. Note that the term "centromeric" used in this context refers to both the centromeric and pericentromeric regions, as they are difficult to distinguish from one another.

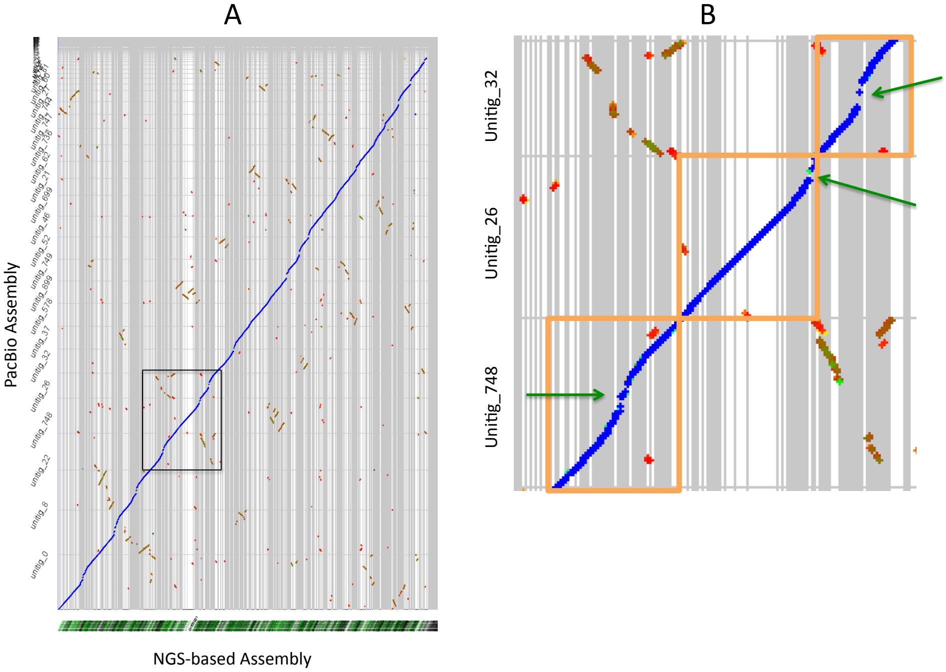

Fig. S6. Syntenic path alignment of the *U. gibba* short-read assembly (x-axis) against the PacBio assembly (y-axis), generated by SynMap in CoGe. Gray vertical and horizontal lines demarcate individual contigs/scaffolds from the short-read and PacBio assemblies, respectively. **(B)** The enlarged detail is encompassed within the black rectangle in **(A)**. Chromosomes are boxed in orange, and it is readily apparent that the x-axis dimensions of these boxes are narrower than their y-axis dimensions, indicating missing DNA in the short-read assembly. Putative centromeric regions lie at gaps in assembly cross-match (highlighted by green arrows), where short scaffolds from the short-read assembly are compacted. Furthermore, the "swooping" syntenic lines composed of homologous gene model matches (blue dots) are caused by the increasing absence of assembled repetitive DNA in the short-read genome toward the centromere (41). Green-red dots illustrate internally syntenic regions of both U. gibba genome assemblies (see section 4 for details).

To further investigate putative centromeric regions, we performed pairwise chromosomal alignments on the four complete chromosomes using MUMmer (42). TE families and other repetitive elements that accumulated in centromeric regions would show increased homology in the pairwise alignment. As expected, the putative centromeric regions were highlighted by increased dot density, whereupon the boundaries of putative centromeres were estimated (Fig. S7). These regions were also confirmed as TE-rich and gene-poor regions through comparison to our repetitive element annotation and gene model prediction pipelines (Fig. S8).

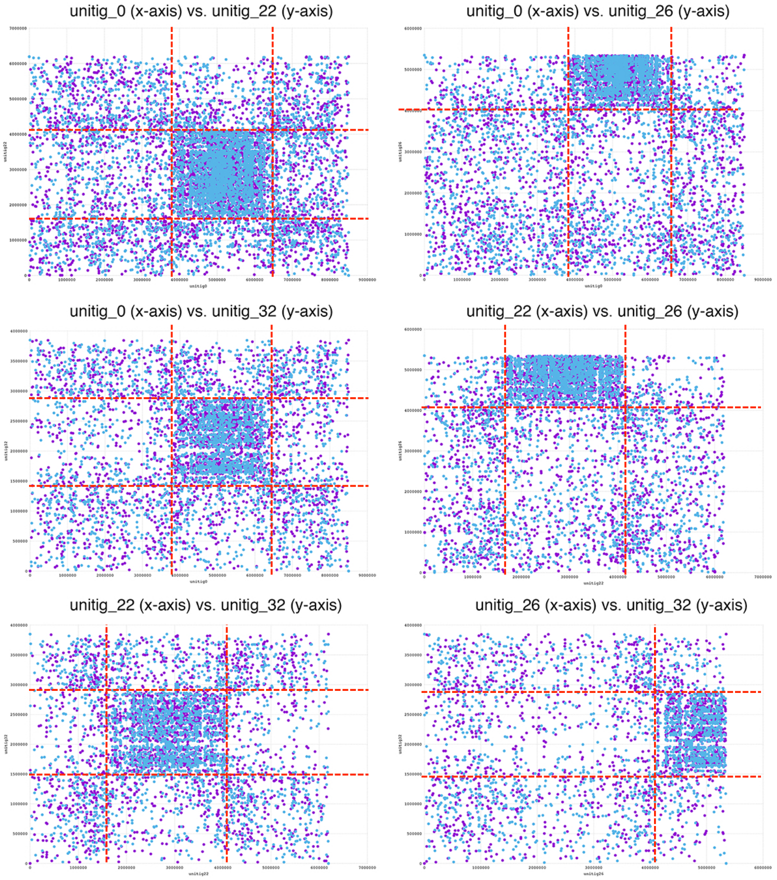

Fig. S7. Pairwise chromosomal alignment plots generated by MUMmer. Red dashed lines indicate the estimated boundaries of putative centromeric/pericentromeric regions.

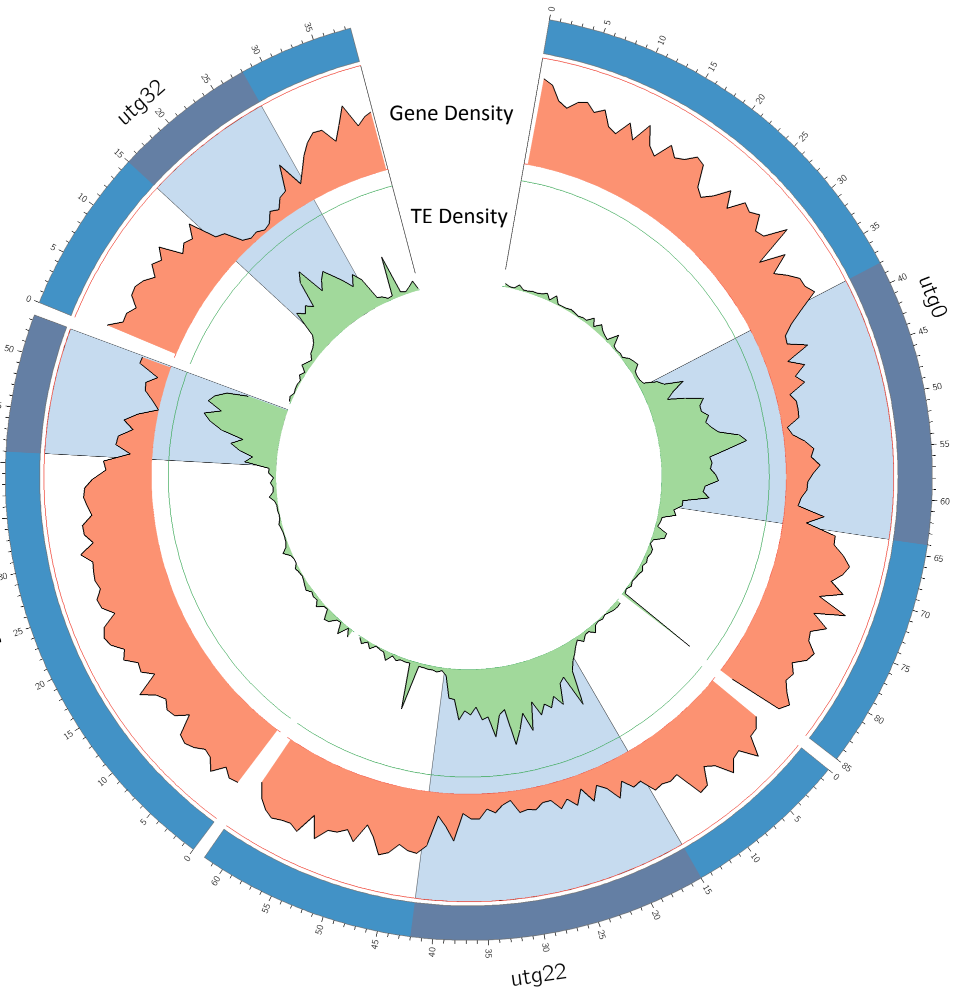

Fig. S8. Visualization of MUMmer-detected putative centromeric regions with TE and gene density tracks in a Circos (43) plot.

3.3.2. Centromeric Repeats Screening

Various arrays of simple tandem repeats are prevalent at the centromeric regions of plant and animal genomes (44-46), yet neither the tandem repeat monomer length nor the repeat sequences are conserved among species that diverged more than 50 MYA (36). In order to identify the signature centromeric repeats in *U. gibba*, tandem repeat clusters with average period size of 50-500 bp were selected for identification as putative centromere repeats (Fig. S5B) as in (36). The top 10 most abundant tandem repeat clusters were considered to be prime candidates for centromeric repeats, but these were not even preferentially located in our chromosome-sized contigs. We then manually checked the locations of the next 10 most abundant tandem repeat clusters in the genome; however, none of these clusters showed unique localization in putative centromeric regions. We thus speculated that *U. gibba* may be devoid of high-copy tandem repeat arrays in its centromeres. Similar findings have also been reported for the centromeres of several plant and animal species (47-49), including two carnivorous plant species, *Genlisea hispidula* and *G. subglabra* (34).

3.3.3. Identification of Putative Centromeric CRM Retrotransposons

While plant retrotransposon families are in general randomly dispersed, there are families distinctly concentrated in centromeric regions. Centromeric retrotransposons, CRMs, which locate preferentially in centromeric regions, are among the latter category. CRM chromoviruses, a lineage of Ty3/gypsy retrotransposons, have been well characterized as centromeric retrotransposons in many species (50-55), including *G. hispidula* and *G. subglabra* (34). CRM elements can be categorized into three subgroups, of which subgroup A and B are concentrated in centromeric regions (56). The RT domain is a reliable component to discriminate CRM elements from other LTR retrotransposons (57, 58).

Our search strategy for CRMs in *U. gibba* was carried out as follows. First, REPET-annotated TE families of *U. gibba* were queried with CRM sequences from 33 species (56) using blastn with an *E*-value threshold of 1E-5. The six resulting hits were processed with LTR_Finder (59), and only one among the six was identified as a full-sized LTR with an intact RT domain. We then searched the entire *U. gibba* genome using the ORF of the RT domain as a query with an *E*-value threshold of 1E-5. The resulting 55 hits distributed on 24 contigs were then extended by 15 kb both upstream and downstream to include the other portions of the LTRs, which were again processed with LTR_Finder for identification of full-sized LTRs and intact RT domains. As a result, 22 hits were identified as full-sized LTRs with an intact RT domain, while 11 hits were identified as full-sized LTRs with an incomplete RT domain, and 22 hits were identified as incomplete LTRs. The protein sequences of the RT ORFs from the 55 *U. gibba* hits and the 33 species were aligned using MUSCLE (60). Phylogenetic analysis based on the alignment was performed using RAxML-HPC BlackBox version 8.2.6 in CIPRES (61) with the GTR substitution model. A total of 1000 bootstrap relicates were conducted to evaluate branch support. In the maximum likelihood tree shown in Fig. S9, all 55 *U. gibba* sequences were grouped within the subgroup A CRMs, which include the centromere-specific CRMs. All but one of the *U. gibba* sequences together form a single, monophyletic CRM subfamily. To investigate the chromosomal localization of the 55 *U. gibba* CRMs, we plotted them on the complete and near-complete chromosomes together with the TE and gene model tracks. As depicted in Fig. 1 (main text), most *U. gibba* CRMs are located in the putative centromeric regions, however not all putative centromeres had CRM elements.

It has been proposed that CRMs may play an important role in stablizing centromere structure and maintaining centromere function (62, 63), while an opposing hypothesis holds that they are merely parasitic and tend to accumulate in recombination-poor centromeric regions to escape negative selection against insertions in distal regions (64). Our finding that the centromeric regions of several chromosomes lack CRMs, together with the finding that they also lack high-copy centromeric tandem repeats, suggests that neither CRMs nor tandem repeats are crucial for maintaining functional centromeres in *U. gibba*.

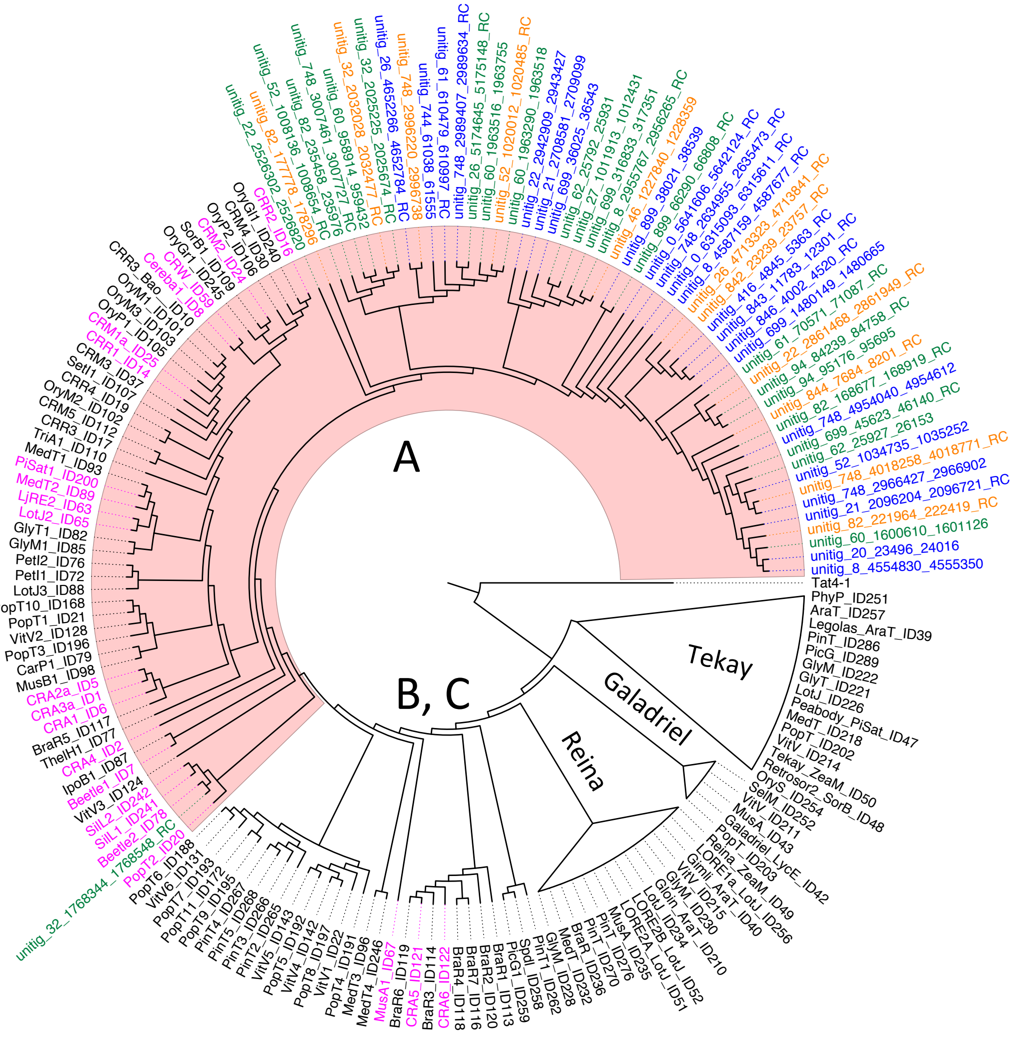

Fig. S9. Phylogenetic reconstruction based on the RAxML analysis of 55 *U. gibba* CRM-like blast hits and CRM reverse transcriptase (RT) domain sequences from (56). CRM subgroup A is highlighted in red. All 55 *U. gibba* sequences grouped with subgroup A CRMs. Full-sized *U. gibba* CRMs predicted by LTR_Finder to have intact RT domains are shown in blue, while the full-sized CRMs with incomplete RT domains and incomplete CRMs are shown in orange and green, respectively. CRM elements with previously confirmed centromeric localization are colored in purple. The collapsed Tekay, Reina and Galadriel clades were included as representatives of other non-CRM plant chromoviruses, and the non-chromovirus element Tat4-1 was used as an outgroup (56).

4. Ancestral Genome Reconstruction and Subgenome Dominance Analysis

4.1. Ancestral Genome Reconstruction

The analysis of the frequency distributions of duplicate gene similarities does not in the first instance involve syntenic considerations. Similarly, the detection of syntenic collinearity does not necessarily depend on similarity other than requiring identified gene pairs to be more similar than a given threshold. But there are many cases where combining the two kinds of data provides a powerful methodology. For example, in attempting to discern the evolution of a genome like *U. gibba* that has undergone at least 2

WGDs, the Ks distribution of similarities created by the more recent event tends to swamp and obscure that from an earlier event (Fig. S10), and the synteny of homeologous chromosomes is degraded, especially for the earlier event, by extensive fractionation and rearrangement.

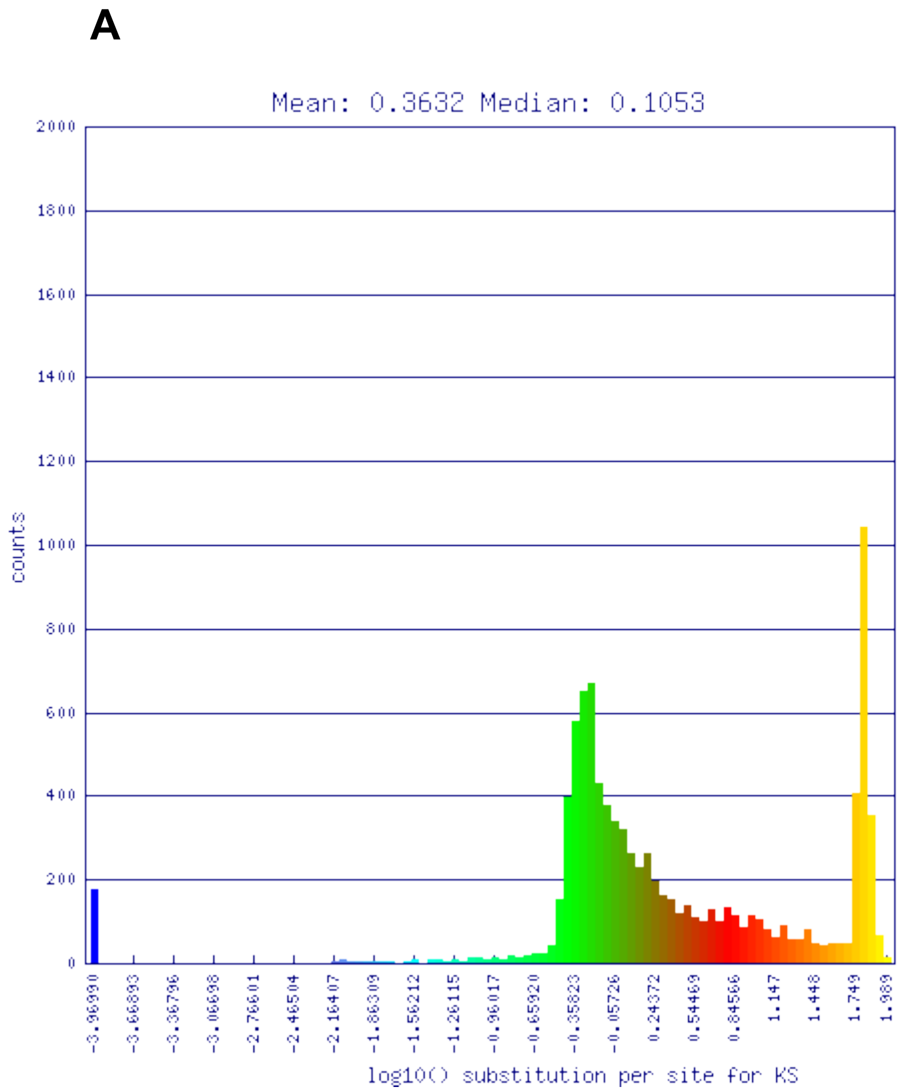

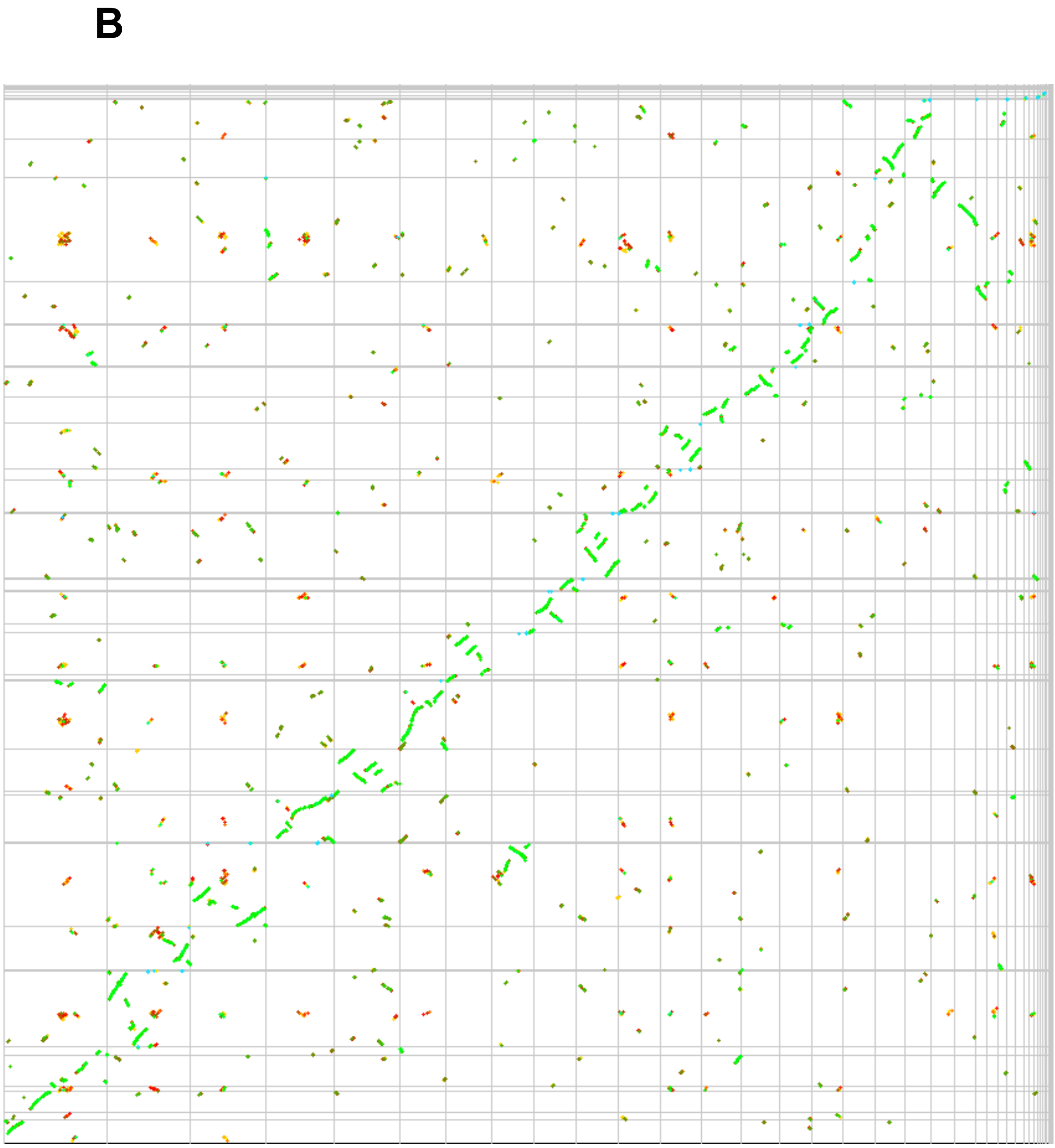

Fig. S10. (A) Distribution of Ks scores of paralogs in *U. gibba*, showing two overlapping distributions, resulting from a recent (light green) WGD event and an earlier (dark green - brown) WGD event. Red paralogous pairs at higher Ks largely represent regions that contain extensive tandemly duplicated genes. Given that Ks reasonably reflects the background (neutral) mutation rate, these red segments (i) may be older than the second-most recent WGD, (ii) they may lie in regions of enhanced mutation rate, or (iii) they may merely represent Ks saturation artifacts (65). Substitutional and insertional mutation rates are known to covary (66), so these regions could be hotspots for both nucleotide mutation and local (tandem) insertional duplication. The yellow peak represents irrational Ks values due to codon misalignments; these are commonly observed in CoGe SynMap results. **(B)** Syntenic dotplot from which **(A)** was derived; the *U. gibba* contigs are ordered with respect to each other (in a syntenic path alignment) such that the syntenic blocks from the most recent WGD event are forced as best possible to the diagonal.

Thus our analysis of WGD in *U. gibba* integrates both kinds of data. The first step is to describe and delimit the most recent event using synteny block construction provided by the SynMap package on the CoGe platform (40, 67), using default values for the parameters, and filtering out gene pairs with Ks outside the interval [-0.6, 0.25]. Neighboring synteny blocks on the same two chromosomes were combined to produce a total of 54 pairs of (larger) blocks, containing 81% of the genes in the genome. These fell into six groupings, where each group contains from one to thirteen homeologous pairs of blocks. Five of these groups consisted essentially of two *U. gibba* chromosomes, either whole or fissioned into two pieces, or containing small translocations (Fig. S11).

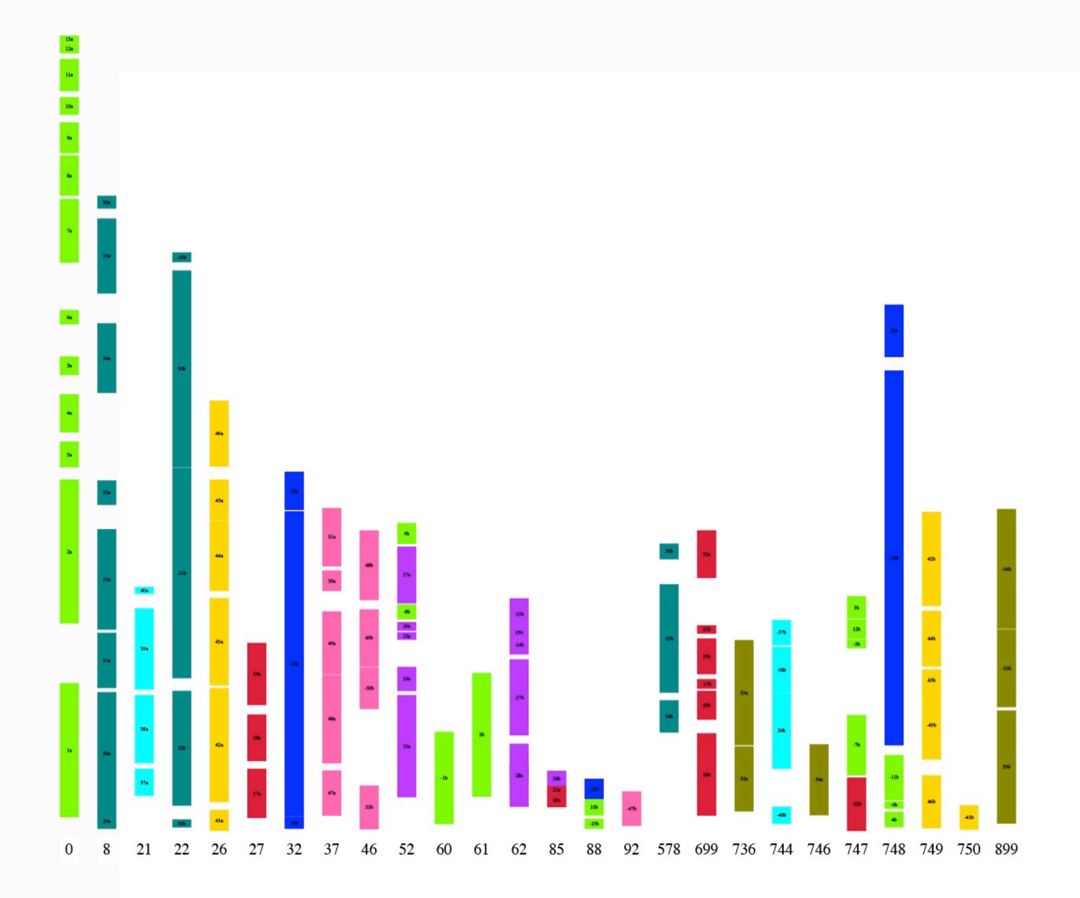

Fig. S11. Nine color-coded homeologous blocks in their current positions in the *U. gibba* karyotype.

In the sixth group, the largest *U. gibba* chromosome can be recognized as a fusion of four ancient chromosomes whose homeologs form all or part of various of the other extant chromosomes. A completely duplicated genome could then be recognized as underlying these nine groups, differing by a small number of readily identified rearrangements (Fig. S12).

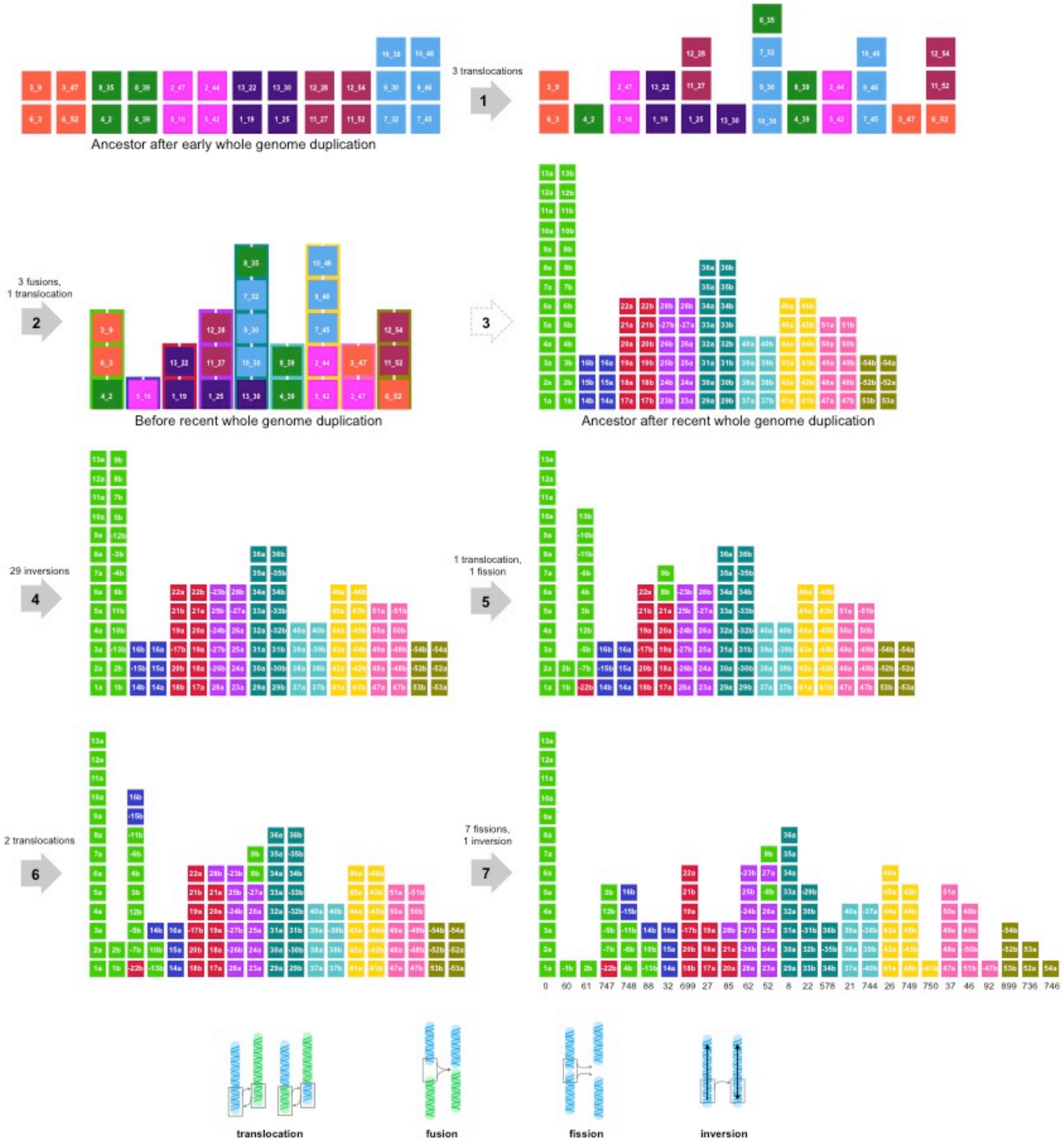

Fig. S12. Reconstruction of *U. gibba* genome structural evolution through two rounds of WGD and subsequent diploidization. Internally syntenic blocks stemming from two ancient polyploidy events were identified in the highly contiguous genome assembly and tracked through multiple translocation, fusion, fission, and especially inversion events (diagramed at bottom) from two ancestral genomes, first an n = 6 chromosome pre-polyploid ancestor, and thereafter an n = 9 ancestor. Panels **(1)-(7)** show the structural rearrangement history of 54 syntenic blocks identified among the modern genome contigs **(7)**, with colors matching ancestral chromosomes. Numbers indicate block identities; “a” versus “b” represents subgenome pairs included in the most recent WGD event, which fractionation and expression and expression data suggest to have been an allopolyploidization. “-“ indicates inverted orientation, and underscore between blocks in the n = 6 ancestor link blocks from the second WGD to those of the first.

In reconstructing the earlier WGD event, we found that the SynMap of the *U. gibba* genome against itself did not produce enough paralogous synteny blocks based on gene pairs with Ks levels around 0.25 or above. Since evolution after speciation retains WGD-generated orthologous pairs to a far greater extent than the paralogous pairs generated by fractionation after WGD, we used a conservative core eudicot genome – *V. vinifera* - to detect 113 sets of separate regions in *U. gibba* syntenic to the same region (or overlapping regions) in *Vitis*. Within each set of regions, for each pair of these regions, we then calculated the average Ks of all the paralogous gene pairs the two of them contained (if any). We then screened all the sets to find any that consisted of quadruples of regions, consisting of two pairs with average similarity clustered around a recent value, representing the recent WGD, where the four (at most) average similarity scores *across* the two pairs of regions were clustered around an earlier value of similarity. (Instability in calculations of average Ks for pairs of regions necessitated the use of an overall similarity measure.) We found 13 quadruples that verified that these conditions; the remaining non-retained sets either contained too many or too few regions, or an insufficient number of paralogous pairs to assess the similarity between all pairs of regions. The quadruples that emerged from this search should be suggestive of the chromosomes produced by the two rounds of WGD, although this may be obscured by rearrangement and fractionation. Using the intermediate ancestral genome as reconstructed in Fig. S12 to represent the more recent WGD, the pattern of common adjacencies in pairs of blocks containing members of different quadruples sufficed to determine a 12-chromosome karyotype resulting from the early WGD.

4.2. Syntenic Block Fractionation Rate Analysis

After reconstructing the amalgamated syntenic blocks and reconstructing their positions on the ancestral karyotype emerging from the recent WGD, we labeled each pair of reconstructed homeologous chromosomes a and b, in no particular order, and compared the fractionation patterns for each pair of homeologous blocks in the two chromosomes, according to the formulae:

$$\text{retention rate in homeolog a} = \frac{\#\text{ genes in a}}{\#\text{ genes in a only} + \#\text{ genes in b only} + \#\text{ genes in both}}$$

$$\text{retention rate in homeolog b} = \frac{\#\text{ genes in b}}{\#\text{ genes in a only} + \#\text{ genes in b only} + \#\text{ genes in both}}$$

The results for the 54 pairs of homeologous blocks, displayed in Fig. S13, show that for eight of the nine chromosome pairs, the blocks in one homeolog have consistently higher retention rates (Dataset S3). This suggests that one of the two subgenomes involved in the WGD was dominant, retaining more genes during fractionation than the other. Indeed, high versus low gene retention rates *within* chromosomes or chromosome-sized contigs (e.g., the light green unitig_0 in Fig. S13) may represent homeologous recombination between subgenomes after the most recent WGD.

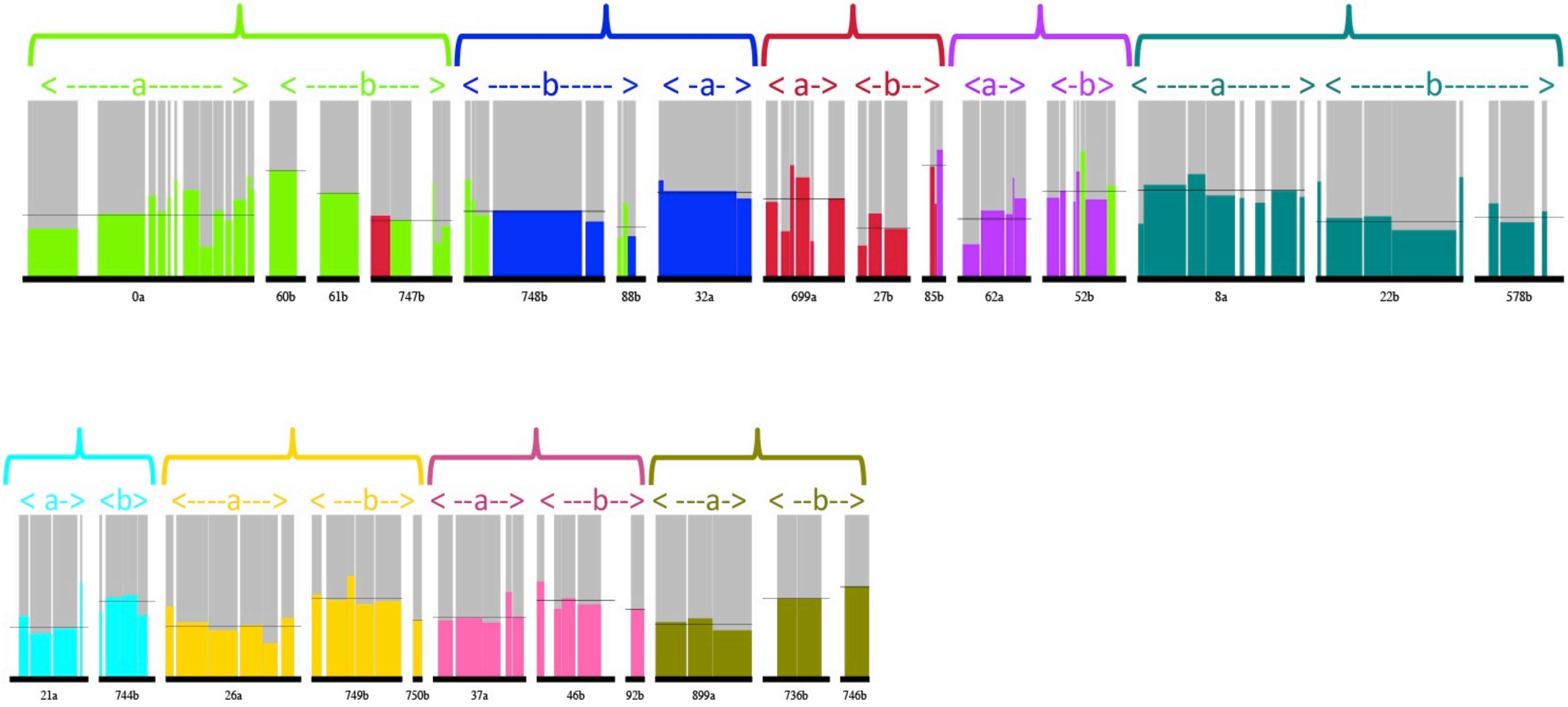

Fig. S13. Fractionation patterns in nine pairs of reconstructed chromosomes, colored according to chromosome, with a versus b subgenome pairs shown and sets of contributing contigs enveloped in brackets (with some interchromosomal rearrangements apparent). Y-axis indicates extent of fractionation, with contig-wise averages shown as dotted lines.

4.3. Subgenome Differential Expression Analysis

To investigate gene expression levels between the two subgenomes, we used raw read counts instead of normalized read counts, since all comparisons were performed within each library. Beside the shoot, trap, and inflorescence libraries, we also included the raw read counts from a stress condition library (27) and the raw read counts from the Ion Torrent RNA-seq reads sequenced from pooled tissues of the whole *U. gibba* plant (NCBI accession SRX247091, from (2)). Homeologs, which are the syntenic gene pairs obtained from SynMap, were assigned to the dominant (less fractionated) or recessive (more fractionated) subgenomes based on their locations within the syntenic blocks. Expression fold change was calculated for each homeolog using the ratio of the read counts in one subgenome versus the other. We considered homeologs to be differentially expressed if they had an expression fold change higher than the cutoff (2, 5, 10, 15, or 20-fold). Comparisons of total dominantly-expressed genes (as occurring either on the dominant or recessive subgenome) are summarized in Fig. S14. A consistent bias was observed (among most datasets and fold cutoffs) whereby the dominant subgenome showed a greater number of dominantly expressed genes. The *p*-values calculated using cumulative binomial distributions were significant at 2-fold expression difference in every transcriptome dataset except the one representing stress conditions. However, as the fold cutoff increased, the biased gene expression dominance in the dominant subgenome became less significant or non-significant. For example, when the fold cutoff was set to 20-fold, the recessive subgenome had a higher number of dominantly expressed genes in shoots.

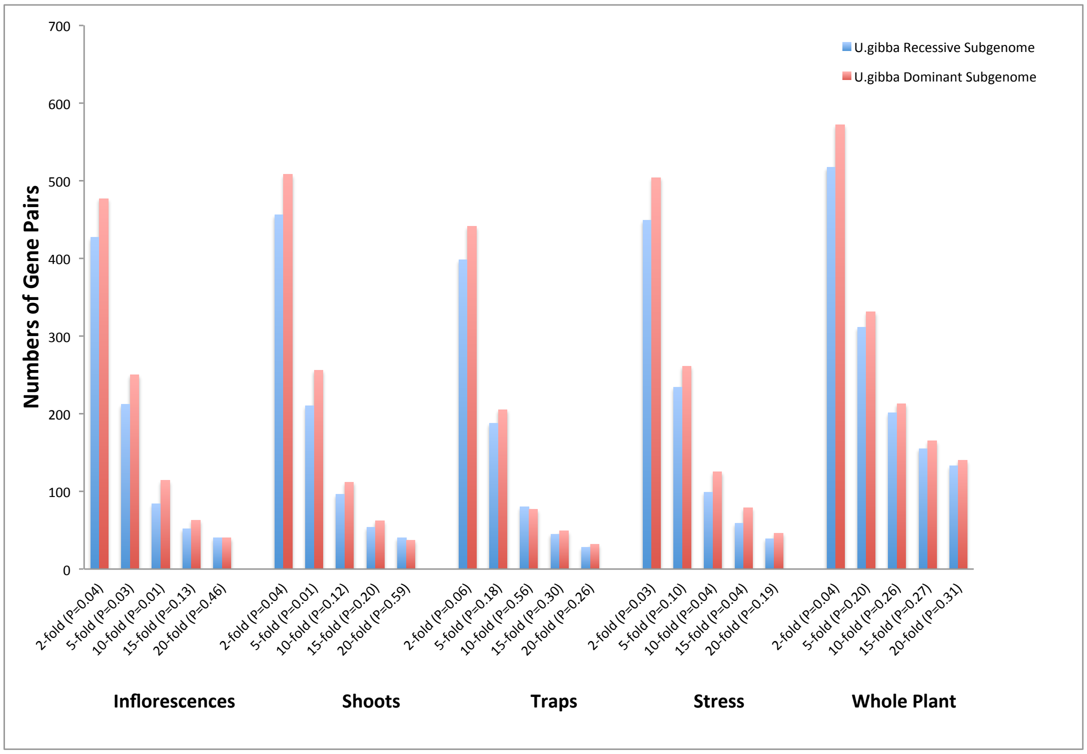

Fig. S14. Patterns of *U. gibba* homeolog expression in shoots, traps, inflorescences and the whole plant. All *p*-values were calculated using cumulative binomial distributions assuming an equal chance of gene copies for the dominant versus recessive subgenome to dominate total expression for the gene pair.

4.4. Variant Calling and Subgenome Heterozygosity Rate Analysis

Illumina and 454 raw reads from our previous short-read assembly (2) were aligned to the PacBio assembly using BWA mem version 0.7.7 (68) with default parameters. The resulting BAM files were filtered using SAMtools version 0.1.19 (69) with option "-q 30" to only keep reads that had mapping quality larger than 30. Duplicated reads created by PCR amplification during library preparation were removed using the MarkDuplicates tool in the Picard software suite version 1.112 (http://broadinstitute.github.io/picard/) with lenient validation stringency. The Illumina- and 454-derived BAM files were then merged using SAMtools. Variant calling was implemented using the HaplotypeCaller tool in the GATK toolkit version 3.2 (70) with default settings. Heterozygous SNPs were then extracted from the resulting VCF file. Heterozygous SNPs were counted within each syntenic block and then added up for all dominant and recessive subgenome blocks, respectively. The heterozygosity rate was calculated as the total number of heterozygous SNPs divided by the total number of nucleotides in the blocks (Dataset S4). The bias ratio was calculated as the heterozygosity rate in the recessive subgenome divided by the rate in the dominant subgenome. The 1.5-times higher heterozygosity rate in the recessive subgenome implies stronger purifying selection acting on the dominant subgenome.

4.5. Whole Genome Duplication Analyses: Examples of Multiple *U. gibba* Blocks Syntenic to *Vitis*

Multiple *U. gibba* blocks in synteny with a single block of the *V. vinifera* genome could suggest either evidence for a third WGD (2) or retained synteny from the paleohexaploidy event that occurred at the base of core eudicots (71). We examined a number of cases of 8:1, or greater than 8:1 syntenic relationships compiled for *U. gibba* versus individual *Vitis* blocks using the SynFind tool (72). We illustrate 9 cases below of such multi-block relationships using CoGe's GEvo tool (Figs. S15-23). In each case, multiple *U. gibba* blocks show intercalated synteny (via block-specific, colored lines connecting BLAST HSPs) against a single *Vitis* block, as would be expected from a minimum of 3 WGD events. However, some of the multiple blocks are likely neighbors of each other instead of existing in complete overlap, since the rearranged structure of the *U. gibba* genome makes the latter status difficult to resolve for old, heavily fractionated duplicate regions. Furthermore, some of the multiple *U. gibba* blocks might instead be best matches to other, triplicated *Vitis* blocks that are homeologous with the query regions shown here; in other words, some of the multiply syntenic *U. gibba* blocks shown could simply date to the paleohexaploidy event. Preliminary analyses suggest that this might be the case for some comparisons, so we reserve judgment for the time being on the existence of a third lineage-specific WGD having occurred during *U. gibba* genome evolution.

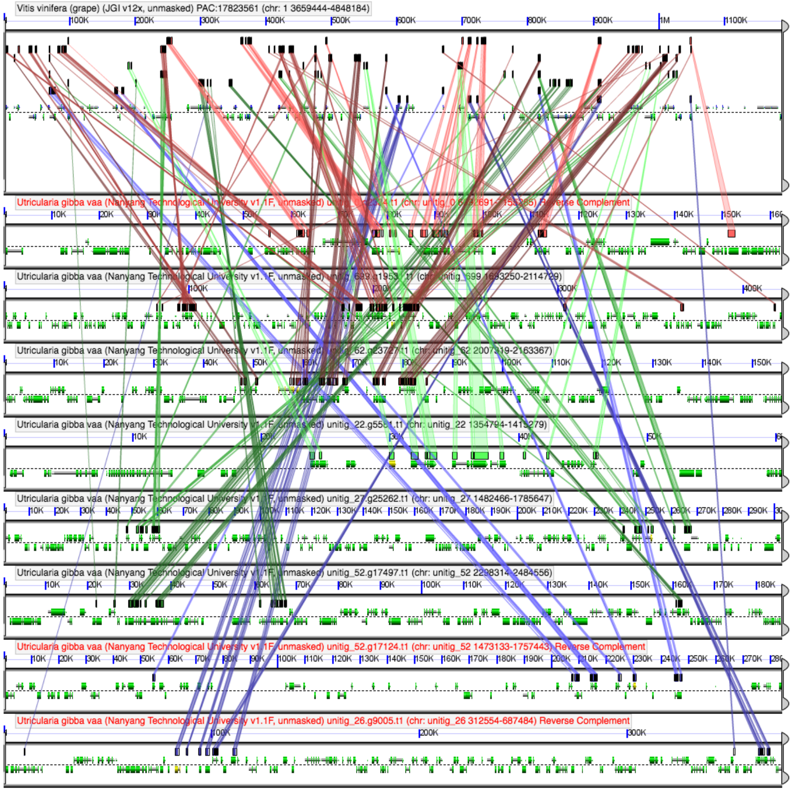

Fig. S15. GEvo plot for *Vitis* chr1. CoGe website link: https://genomevolution.org/coge//GEvo.pl?prog=blastz;iw=1000;fh=10;padding=1;hsp_top=1;nt=0;cbc=0;spike_len=15;ca=1;skip_feat_overlap=1;skip_hsp_overlap=1;hs=0;bzW=8;bzK=3000;bzO=400;bzE=30;accn1=PAC%3A17823561;fid1=391283430;dsid1=80882;dsgid1=19990;chr1=1;dr1up=492308;dr1down=693716;ref1=1;mask1=non-cds;accn2=unitig_0.g2334.t1;fid2=826717306;dsid2=98983;dsgid2=28800;chr2=unitig_0;dr2up=80000;dr2down=80000;rev2=1;ref2=0;mask2=non-cds;accn3=unitig_699.g19531.t1;fid3=826753816;dsid3=98983;dsgid3=28800;chr3=unitig_699;dr3up=210000;dr3down=210000;ref3=0;mask3=non-cds;accn4=unitig_62.g23727.t1;fid4=826750848;dsid4=98983;dsgid4=28800;chr4=unitig_62;dr4up=55130;dr4down=96624;ref4=0;mask4=non-cds;accn5=unitig_22.g5581.t1;fid5=826725416;dsid5=98983;dsgid5=28800;chr5=unitig_22;dr5up=30000;dr5down=30000;ref5=0;mask5=non-cds;accn6=unitig_27.g25262.t1;fid6=826732448;dsid6=98983;dsgid6=28800;chr6=unitig_27;dr6up=250000;dr6down=50266;ref6=0;mask6=non-cds;accn7=unitig_52.g17497.t1;fid7=826743884;dsid7=98983;dsgid7=28800;chr7=unitig_52;dr7up=359615;dr7down=-175926;ref7=0;mask7=non-cds;accn8=unitig_52.g17124.t1;fid8=826743204;dsid8=98983;dsgid8=28800;chr8=unitig_52;dr8up=230000;dr8down=53025;rev8=1;ref8=0;mask8=non-cds;accn9=unitig_26.g9005.t1;fid9=826729650;dsid9=98983;dsgid9=28800;chr9=unitig_26;dr9up=82680;dr9down=290000;rev9=1;ref9=0;mask9=non-cds;num_seqs=9;hsp_overlap_limit=0;hsp_size_limit=0

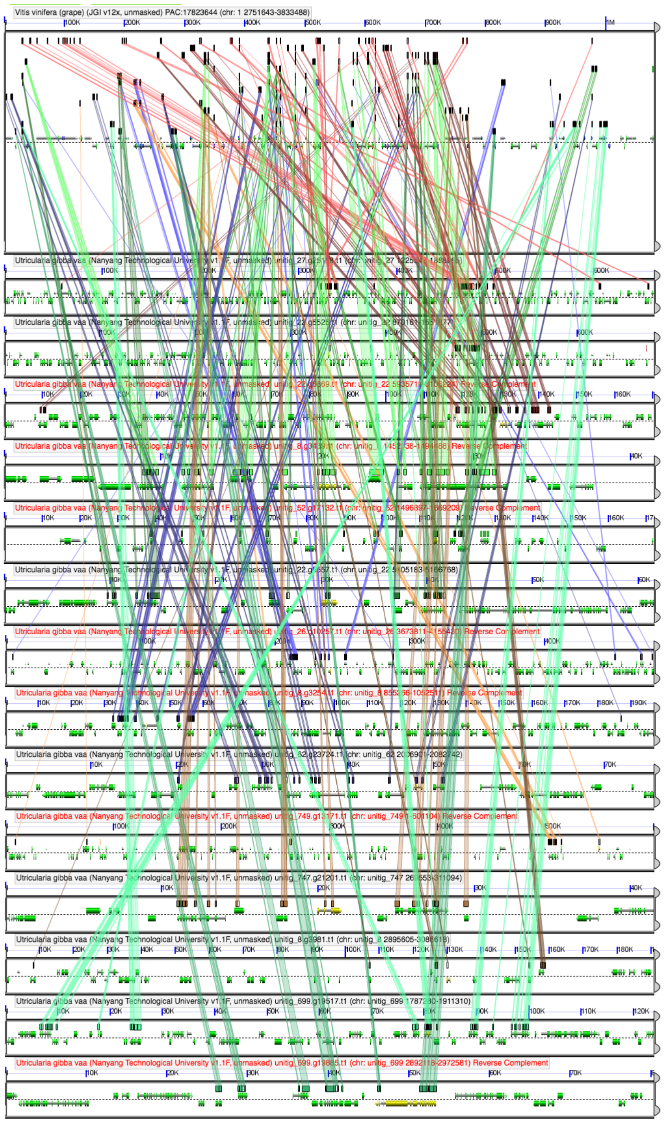

Fig. S16. A second GEvo plot for *Vitis* chr1. CoGe website link: https://genomevolution.org/coge//GEvo.pl?prog=blastz;iw=1000;fh=10;padding=1;hsp_top=1;nt=0;cbc=0;spike_len=15;ca=1;skip_feat_overlap=1;skip_hsp_overlap=1;hs=0;bzW=8;bzK=3000;bzO=400;bzE=30;accn1=PAC%3A17823644;fid1=391283596;dsid1=80882;dsgid1=19990;chr1=1;dr1up=514180;dr1down=563491;ref1=1;mask1=non-cds;accn2=unitig_27.g25188.t1;fid2=826732302;dsid2=98983;dsgid2=28800;chr2=unitig_27;dr2up=330000;dr2down=330000;ref2=0;mask2=non-cds;accn3=unitig_22.g5525.t1;fid3=826725320;dsid3=98983;dsgid3=28800;chr3=unitig_22;dr3up=340000;dr3down=340000;ref3=0;mask3=non-cds;accn4=unitig_22.g6869.t1;fid4=826727502;dsid4=98983;dsgid4=28800;chr4=unitig_22;dr4up=130000;dr4down=38731;rev4=1;ref4=0;mask4=non-cds;accn5=unitig_8.g3439.t1;fid5=826767652;dsid5=98983;dsgid5=28800;chr5=unitig_8;dr5up=20000;dr5down=20000;rev5=1;ref5=0;mask5=non-cds;accn6=unitig_52.g17132.t1;fid6=826743220;dsid6=98983;dsgid6=28800;chr6=unitig_52;dr6up=113792;dr6down=57483;rev6=1;ref6=0;mask6=non-cds;accn7=unitig_22.g6557.t1;fid7=826726924;dsid7=98983;dsgid7=28800;chr7=unitig_22;dr7up=30000;dr7down=30000;ref7=0;mask7=non-cds;accn8=unitig_26.g10257.t1;fid8=826728790;dsid8=98983;dsgid8=28800;chr8=unitig_26;dr8up=240000;dr8down=240000;rev8=1;ref8=0;mask8=non-cds;accn9=unitig_8.g3254.t1;fid9=826767318;dsid9=98983;dsgid9=28800;chr9=unitig_8;dr9up=43178;dr9down=15000

0;rev9=1;ref9=0;mask9=non-cds;accn10=unitig_62.g23724.t1;fid10=826750844;dsid10=98983;dsgid10=28800;chr10=unitig_62;dr10up=47761;dr10down=26965;ref10=0;mask10=non-cds;accn11=unitig_749.g13171.t1;fid11=826763646;dsid11=98983;dsgid11=28800;chr11=unitig_749;dr11up=550000;dr11down=550000;rev11=1;ref11=0;mask11=non-cds;accn12=unitig_747.g21201.t1;fid12=826759016;dsid12=98983;dsgid12=28800;chr12=unitig_747;dr12up=20000;dr12down=20000;ref12=0;mask12=non-cds;accn13=unitig_8.g3981.t1;fid13=826768650;dsid13=98983;dsgid13=28800;chr13=unitig_8;dr13up=130000;dr13down=60016;ref13=0;mask13=non-cds;accn14=unitig_699.g19517.t1;fid14=826753788;dsid14=98983;dsgid14=28800;chr14=unitig_699;dr14up=80000;dr14down=42608;ref14=0;mask14=non-cds;accn15=unitig_699.g19885.t1;fid15=826754494;dsid15=98983;dsgid15=28800;chr15=unitig_699;dr15up=45909;dr15down=27029;rev15=1;ref15=0;mask15=non-cds;num_seqs=15;hsp_overlap_limit=0;hsp_size_limit=0

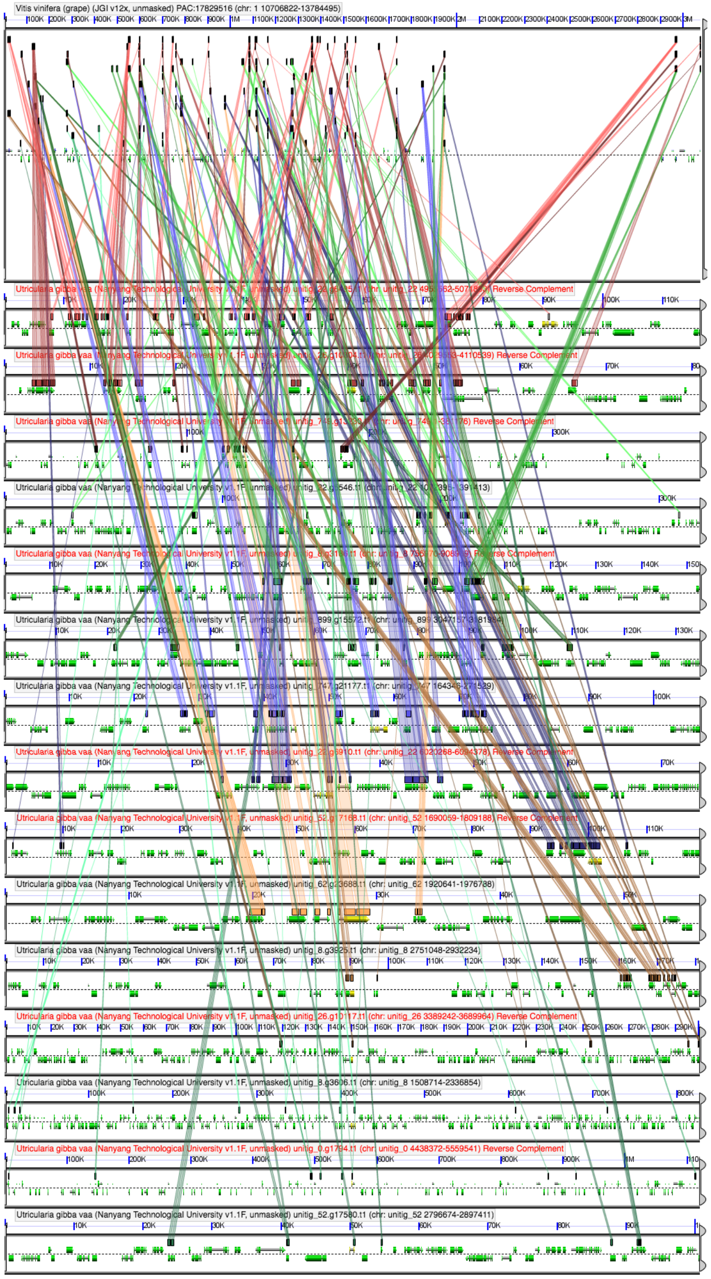
Vitis vinifera (grape) (JGI v12x, unmasked) PAC:17829516 (chr: 1 10706822-13784495)
Utricularia gibba vaa (Nanyang Technological University v1.1F, unmasked) unitig_22 (chr: unitig_22) Reverse Complement
Utricularia gibba vaa (Nanyang Technological University v1.1F, unmasked) unitig_26 (chr: unitig_26 -4110539) Reverse Complement
Utricularia gibba vaa (Nanyang Technological University v1.1F, unmasked) unitig_749 (chr: unitig_749) Reverse Complement
Utricularia gibba vaa (Nanyang Technological University v1.1F, unmasked) unitig_22.g546.t1 (chr: unitig_22)
Utricularia gibba vaa (Nanyang Technological University v1.1F, unmasked) unitig_8 (chr: unitig_8) Reverse Complement
Utricularia gibba vaa (Nanyang Technological University v1.1F, unmasked) unitig_899.g15572.t1 (chr: unitig_899 3047157-3181984)
Utricularia gibba vaa (Nanyang Technological University v1.1F, unmasked) unitig_747.g21177.t1 (chr: unitig_747 164346-271529)
Utricularia gibba vaa (Nanyang Technological University v1.1F, unmasked) unitig_22.g6910.t1 (chr: unitig_22 6020268-6094378) Reverse Complement
Utricularia gibba vaa (Nanyang Technological University v1.1F, unmasked) unitig_52.g17168.t1 (chr: unitig_52 1690059-1809188) Reverse Complement
Utricularia gibba vaa (Nanyang Technological University v1.1F, unmasked) unitig_62.g23688.t1 (chr: unitig_62 1920641-1976788)
Utricularia gibba vaa (Nanyang Technological University v1.1F, unmasked) unitig_8.g3925.t1 (chr: unitig_8 2751048-2932234)
Utricularia gibba vaa (Nanyang Technological University v1.1F, unmasked) unitig_26.g10117.t1 (chr: unitig_26 3389242-3689964) Reverse Complement
Utricularia gibba vaa (Nanyang Technological University v1.1F, unmasked) unitig_8.g3606.t1 (chr: unitig_8 1508714-2336854)
Utricularia gibba vaa (Nanyang Technological University v1.1F, unmasked) unitig_0.g1794.t1 (chr: unitig_0 4438372-5559541) Reverse Complement
Utricularia gibba vaa (Nanyang Technological University v1.1F, unmasked) unitig_52.g17580.t1 (chr: unitig_52 2796674-2897411)

Fig. S17. A third GEvo plot for *Vitis* chr1. CoGe website link: https://genomevolution.org/coge//GEvo.pl?prog=blastz;iw=1000;fh=10;padding=1;hsp_top=1;nt=0;cbc=0;spike_len=15;ca=1;skip_feat_overlap=1;skip_hsp_overlap=1;hs=0;bzW=8;bzK=3000;bzO=400;bzE=30;accn1=PAC%3A17829516;fid1=391284504;dsid1=80882;dsgid1=19990;chr1=1;dr1up=1050824;dr1down=2018316;ref1=1;mask1=non-cds;accn2=unitig_22.g6495.t1;fid2=826726810;dsid2=98983;dsgid2=28800;chr2=unitig_22;dr2up=90000;dr2down=23729;rev2=1;ref2=0;mask2=non-cds;accn3=unitig_26.g10304.t1;fid3=826728872;dsid3=98983;dsgid3=28800;chr3=unitig_26;dr3up=40000;dr3down=40000;rev3=1;ref3=0;mask3=non-cds;accn4=unitig_749.g13230.t1;fid4=826763712;dsid4=98983;dsgid4=28800;chr4=unitig_749;dr4up=125300;dr4down=390000;rev4=1;ref4=0;mask4=non-cds;accn5=unitig_22.g5546.t1;fid5=826725356;dsid5=98983;dsgid5=28800;chr5=unitig_22;dr5up=202210;dr5down=114874;ref5=0;mask5=non-cds;accn6=unitig_8.g3186.t1;fid6=826767192;dsid6=98983;dsgid6=28800;chr6=unitig_8;dr6up=113043;dr6down=37263;rev6=1;ref6=0;mask6=non-cds;accn7=unitig_899.g15572.t1;fid7=826775122;dsid7=98983;dsgid7=28800;chr7=unitig_899;dr7up=196672;dr7down=-62580;ref7=0;mask7=non-cds;accn8=unitig_747.g21177.t1;fid8=826758972;dsid8=98983;dsgid8=28800;chr8=unitig_747;dr8up=56312;dr8down=48122;ref8=0;mask8=non-cds;accn9=unitig_22.g6910.t1;fid9=826727576;dsid9=98983;dsgid9=28800;chr9=unitig_22;dr9up=32913;dr9down=39193;rev9=1;ref9=0;mask9=non-cds;accn10=unitig_52.g17168.t1;fid10=826743284;dsid10=98983;dsgid10=28800;chr10=unitig_52;dr10up=100000;dr10down=16785;rev10=1;ref10=0;mask10=non-cds;accn11=unitig_62.g23688.t1;fid11=826750774;dsid11=98983;dsgid11=28800;chr11=unitig_62;dr11up=26924;dr11down=26669;ref11=0;mask11=non-cds;accn12=unitig_8.g3925.t1;fid12=826768558;dsid12=98983;dsgid12=28800;chr12=unitig_8;dr12up=90000;dr12down=90000;ref12=0;mask12=non-cds;accn13=unitig_26.g10117.t1;fid13=826728526;dsid13=98983;dsgid13=28800;chr13=unitig_26;dr13up=150000;dr13down=150000;rev13=1;ref13=0;mask13=non-cds;accn14=unitig_8.g3606.t1;fid14=826767972;dsid14=98983;dsgid14=28800;chr14=unitig_8;dr14up=410000;dr14down=410000;ref14=0;mask14=non-cds;accn15=unitig_0.g1794.t1;fid15=826716354;dsid15=98983;dsgid15=28800;chr15=unitig_0;dr15up=560000;dr15down=560000;rev15=1;ref15=0;mask15=non-cds;accn16=unitig_52.g17580.t1;fid16=826744032;dsid16=98983;dsgid16=28800;chr16=unitig_52;dr16up=50000;dr16down=50000;ref16=0;mask16=non-cds;num_seqs=16;hsp_overlap_limit=0;hsp_size_limit=0

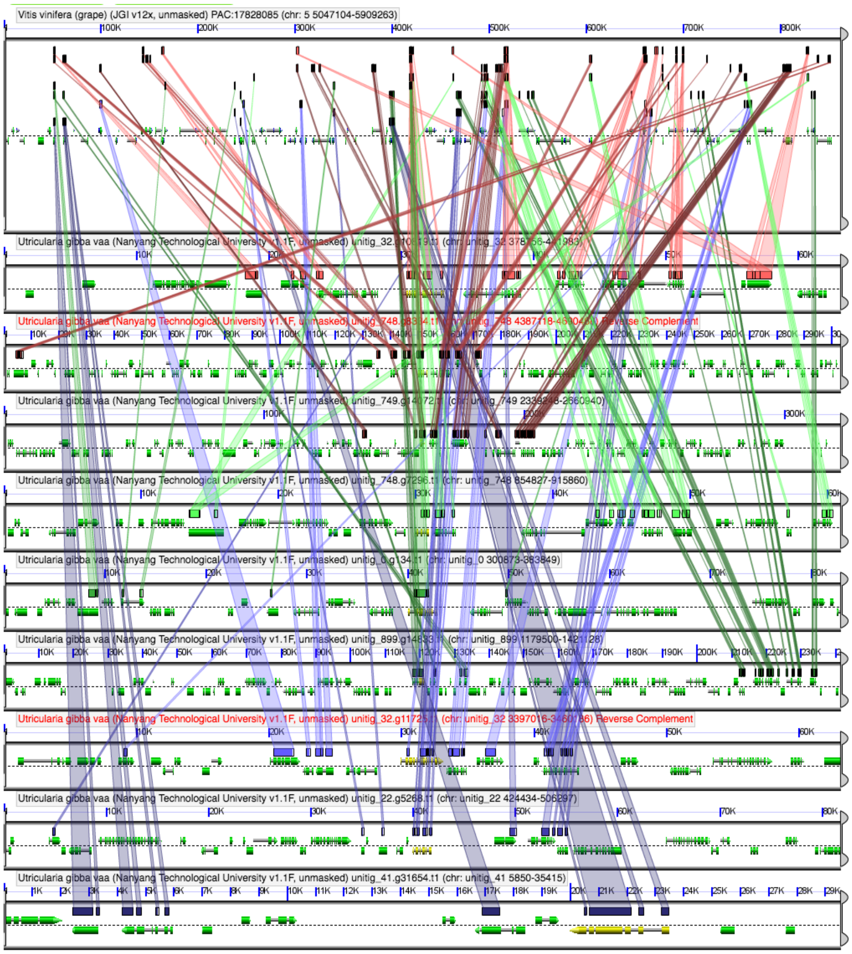

Fig. S18. GEvo plot for *Vitis* chr5. CoGe website link:
https://genomevolution.org/coge//GEvo.pl?prog=blastz;iw=1000;fh=10;padding=1;hsp_top=1;nt=0;cbc=0;spike_len=15;ca=1;skip_feat_overlap=1;skip_hsp_overlap=1;hs=0;bzW=8;bzK=3000;bzO=400;bzE=30;accn1=PAC%3A17828085;fid1=391335607;dsid1=80882;dsgid1=19990;chr1=5;dr1up=417852;dr1down=440698;ref1=1;mask1=non-cds;accn2=unitig_32.g10819.t1;fid2=826734252;dsid2=98983;dsgid2=28800;chr2=unitig_32;dr2up=30000;dr2down=30000;ref2=0;mask2=non-cds;accn3=unitig_748.g8334.t1;fid3=826762842;dsid3=98983;dsgid3=28800;chr3=unitig_748;dr3up=150000;dr3down=150000;rev3=1;ref3=0;mask3=non-cds;accn4=unitig_749.g14072.t1;fid4=826765200;dsid4=98983;dsgid4=28800;chr4=unitig_749;dr4up=160000;dr4down=160000;ref4=0;mask4=non-cds;accn5=unitig_748.g7296.t1;fid5=826761188;dsid5=98983;dsgid5=28800;chr5=unitig_748;dr5up=30000;dr5down=30000;ref5=0;mask5=non-cds;accn6=unitig_0.g134.t1;fid6=826715556;dsid6=98983;dsgid6=28800;chr6=unitig_0;dr6up=40000;dr6down=40000;ref6=0;mask6=non-cds;accn7=unitig_899.g14833.t1;fid7=826773746;dsid7=98983;dsgid7=28800;chr7=unitig_899;dr7up=120000;dr7down=120000;ref7=0;mask7=non-cds;accn8=unitig_32.g11725.t1;fid8=826735616;dsid8=98983;dsgid8=28800;chr8=unitig_32;dr8up=30000;dr8down=30000;rev8=1;ref8=0;mask8=non-cds;accn9=unitig_22.g5268.t1;fid9=826724862;dsid9=98983;dsgid9=28800;chr9=unitig_22;dr9up=40000;dr9down=40000;ref9=0;mask9=non-cds;accn10=unitig_41.g31654.t1;fid10=826738952;dsid10=98983;dsgid10=28800;chr10=unitig_41;dr10up=20000;dr10down=20000;ref10=0;mask10=non-cds;num_seqs=10;hsp_overlap_limit=0;hsp_size_limit=0

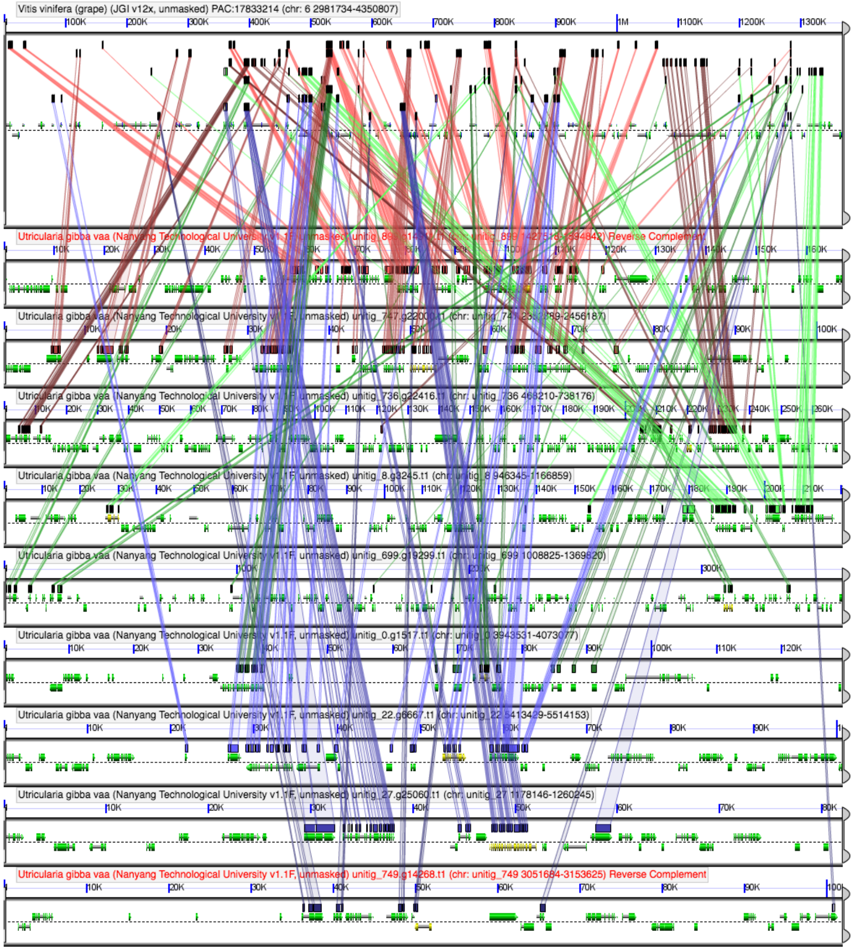

Fig. S19. GEvo plot for *Vitis* chr6. CoGe website link: https://genomevolution.org/coge//GEvo.pl?prog=blastz;iw=1000;fh=10;padding=1;hsp_top=1;nt=0;cbc=0;spike_len=15;ca=1;skip_feat_overlap=1;skip_hsp_overlap=1;hs=0;bzW=8;bzK=3000;bzO=400;bzE=30;accn1=PAC%3A17833214;fid1=391339802;dsid1=80882;dsgid1=19990;chr1=6;dr1up=783997;dr1down=575518;ref1=1;mask1=non-cds;accn2=unitig_899.g14911.t1;fid2=826773892;dsid2=98983;dsgid2=28800;chr2=unitig_899;dr2up=101933;dr2down=62295;rev2=1;ref2=0;mask2=non-cds;accn3=unitig_747.g22000.t1;fid3=826760454;dsid3=98983;dsgid3=28800;chr3=unitig_747;dr3up=50000;dr3down=50000;ref3=0;mask3=non-cds;accn4=unitig_736.g22416.t1;fid4=826755688;dsid4=98983;dsgid4=28800;chr4=unitig_736;dr4up=220000;dr4down=48535;ref4=0;mask4=non-cds;accn5=unitig_8.g3245.t1;fid5=826767304;dsid5=98983;dsgid5=28800;chr5=unitig_8;dr5up=26856;dr5down=190000;ref5=0;mask5=non-cds;accn6=unitig_699.g19299.t1;fid6=826753386;dsid6=98983;dsgid6=28800;chr6=unitig_699;dr6up=310000;dr6down=47365;ref6=0;mask6=non-cds;accn7=unitig_0.g1517.t1;fid7=826715922;dsid7=98983;dsgid7=28800;chr7=unitig_0;dr7up=73562;dr7down=54442;ref7=0;mask7=non-cds;accn8=unitig_22.g6667.t1;fid8=826727126;dsid8=98983;dsgid8=28800;chr8=unitig_22;dr8up=52725;dr8down=45212;ref8=0;mask8=non-cds;accn9=unitig_27.g25060.t1;fid9=826732068;dsid9=98983;dsgid9=28800;chr9=unitig_27;dr9up=47565;dr9down=29997;ref9=0;mask9=non-cds;accn10=unitig_749.g14268.t1;fid10=826765562;dsid10=98983;dsgid10=28800;chr10=unitig_749;dr10up=50000;dr10down=50000;rev10=1;ref10=0;mask10=non-cds;num_seqs=10;hsp_overlap_limit=0;hsp_size_limit=0

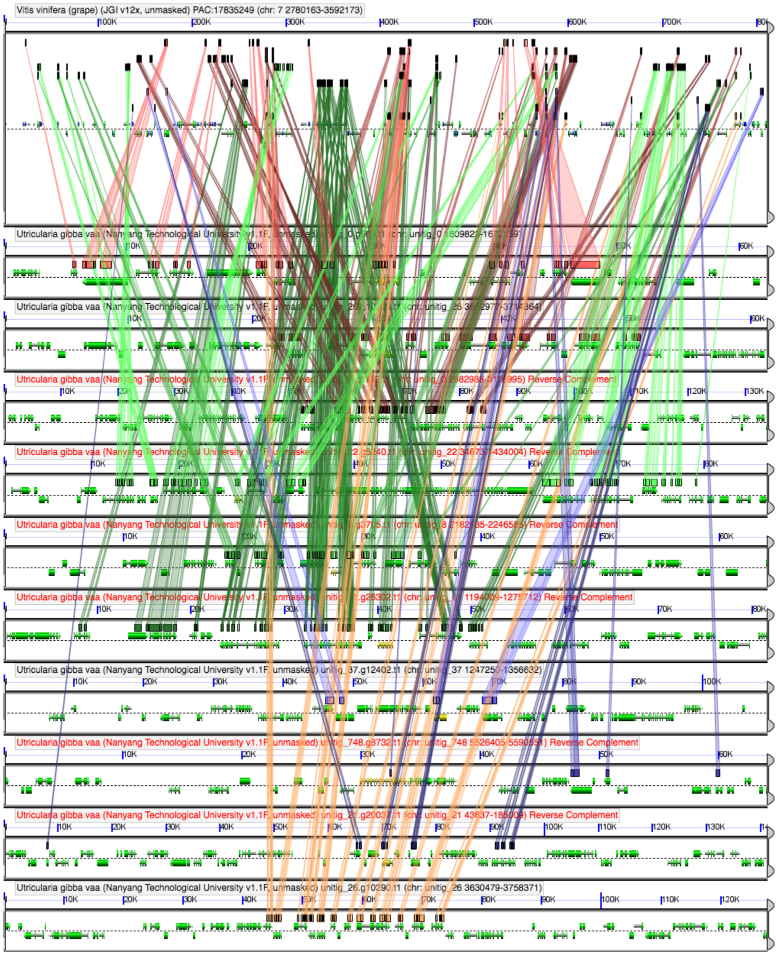

Fig. S20. GEvo plot for *Vitis* chr7. CoGe website link: https://genomevolution.org/coge//GEvo.pl?prog=blastz;iw=1000;fh=10;padding=1;hsp_top=1;nt=0;cbc=0;spike_len=15;ca=1;skip_feat_overlap=1;skip_hsp_overlap=1;hs=0;bzW=8;bzK=3000;bzO=400;bzE=30;accn1=PAC%3A17835249;fid1=391344373;dsid1=80882;dsgid1=19990;chr1=7;dr1up=429973;dr1down=378851;ref1=1;mask1=non-cds;accn2=unitig_0.g664.t1;fid2=826719196;dsid2=98983;dsgid2=28800;chr2=unitig_0;dr2up=30000;dr2down=30000;ref2=0;mask2=non-cds;accn3=unitig_26.g10173.t1;fid3=826728634;dsid3=98983;dsgid3=28800;chr3=unitig_26;dr3up=30000;dr3down=30000;ref3=0;mask3=non-cds;accn4=unitig_0.g1172.t1;fid4=826715220;dsid4=98983;dsgid4=28800;chr4=unitig_0;dr4up=69448;dr4down=63269;rev4=1;ref4=0;mask4=non-cds;accn5=unitig_22.g5240.t1;fid5=826724808;dsid5=98983;dsgid5=28800;chr5=unitig_22;dr5up=26358;dr5down=60000;rev5=1;ref5=0;mask5=non-cds;accn6=unitig_8.g3705.t1;fid6=826768160;dsid6=98983;dsgid6=28800;chr6=unitig_8;dr6up=27467;dr6down=35647;rev6=1;ref6=0;mask6=non-cds;accn7=unitig_61.g26302.t1;fid7=826749334;dsid7=98983;dsgid7=28800;chr7=unitig_61;dr7up=40000;dr7down=40000;rev7=1;ref7=0;mask7=non-cds;accn8=unitig_37.g12402.t1;fid8=826737194;dsid8=98983;dsgid8=28800;chr8=unitig_37;dr8up=61633;dr8down=45978;ref8=0;mask8=non-cds;accn9=unitig_748.g8732.t1;fid9=826763546;dsid9=98983;dsgid9=28800;chr9=unitig_748;dr9up=30000;dr9down=30000;rev9=1;ref9=0;mask9=non-cds;accn10=unitig_21.g20037.t1;fid10=826722446;dsid10=98983;dsgid10=28800;chr10=unitig_21;dr10up=70000;dr10down=70000;rev10=1;ref10=0;mask10=non-cds;accn11=unitig_26.g10290.t1;fid11=826728848;dsid11=98983;dsgid11=28800;chr11=unitig_26;dr11up=401283;dr11down=-275819;ref11=0;mask11=non-cds;num_seqs=11;hsp_overlap_limit=0;hsp_size_limit=0

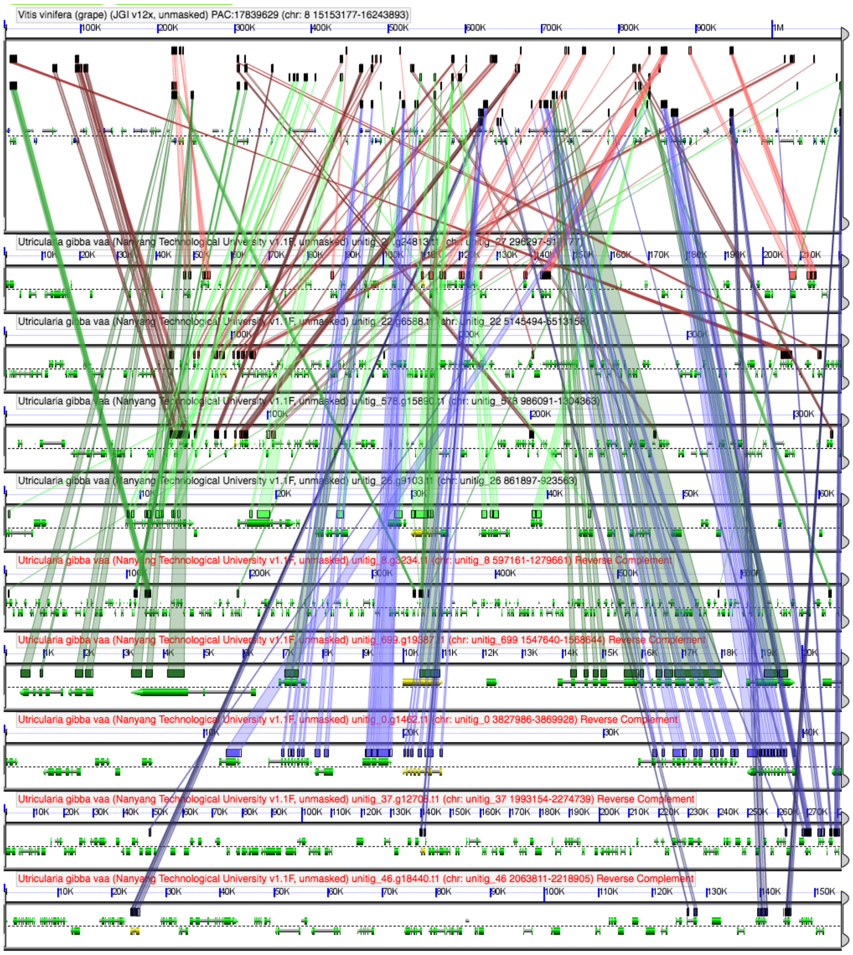

Fig. S21. GEvo plot for *Vitis* chr8. CoGe website link: https://genomevolution.org/coge//GEvo.pl?prog=blastz;iw=1000;fh=10;padding=1;hsp_top=1;nt=0;cbc=0;spike_len=15;ca=1;skip_feat_overlap=1;skip_hsp_overlap=1;hs=0;bzW=8;bzK=3000;bzO=400;bzE=30;accn1=PAC%3A17839629;fid1=391349808;dsid1=80882;dsgid1=19990;chr1=8;dr1up=583528;dr1down=504151;ref1=1;mask1=non-cds;accn2=unitig_27.g24813.t1;fid2=826731654;dsid2=98983;dsgid2=28800;chr2=unitig_27;dr2up=110000;dr2down=110000;ref2=0;mask2=non-cds;accn3=unitig_22.g6588.t1;fid3=826726980;dsid3=98983;dsgid3=28800;chr3=unitig_22;dr3up=94971;dr3down=270000;ref3=0;mask3=non-cds;accn4=unitig_578.g15890.t1;fid4=826746028;dsid4=98983;dsgid4=28800;chr4=unitig_578;dr4up=87539;dr4down=230000;ref4=0;mask4=non-cds;accn5=unitig_26.g9103.t1;fid5=826729826;dsid5=98983;dsgid5=28800;chr5=unitig_26;dr5up=30000;dr5down=30000;ref5=0;mask5=non-cds;accn6=unitig_8.g3234.t1;fid6=826767284;dsid6=98983;dsgid6=28800;chr6=unitig_8;dr6up=340000;dr6down=340000;rev6=1;ref6=0;mask6=non-cds;accn7=unitig_699.g19387.t1;fid7=826753542;dsid7=98983;dsgid7=28800;chr7=unitig_699;dr7up=10000;dr7down=10000;rev7=1;ref7=0;mask7=non-cds;accn8=unitig_0.g1462.t1;fid8=826715810;dsid8=98983;dsgid8=28800;chr8=unitig_0;dr8up=20000;dr8down=20000;rev8=1;ref8=0;mask8=non-cds;accn9=unitig_37.g12708.t1;fid9=826737746;dsid9=98983;dsgid9=28800;chr9=unitig_37;dr9up=140000;dr9down=140000;rev9=1;ref9=0;mask9=non-cds;accn10=unitig_46.g18440.t1;fid10=826741104;dsid10=98983;dsgid10=28800;chr10=unitig_46;dr10up=23540;dr10down=130000;rev10=1;ref10=0;mask10=non-cds;num_seqs=10;hsp_overlap_limit=0;hsp_size_limit=0

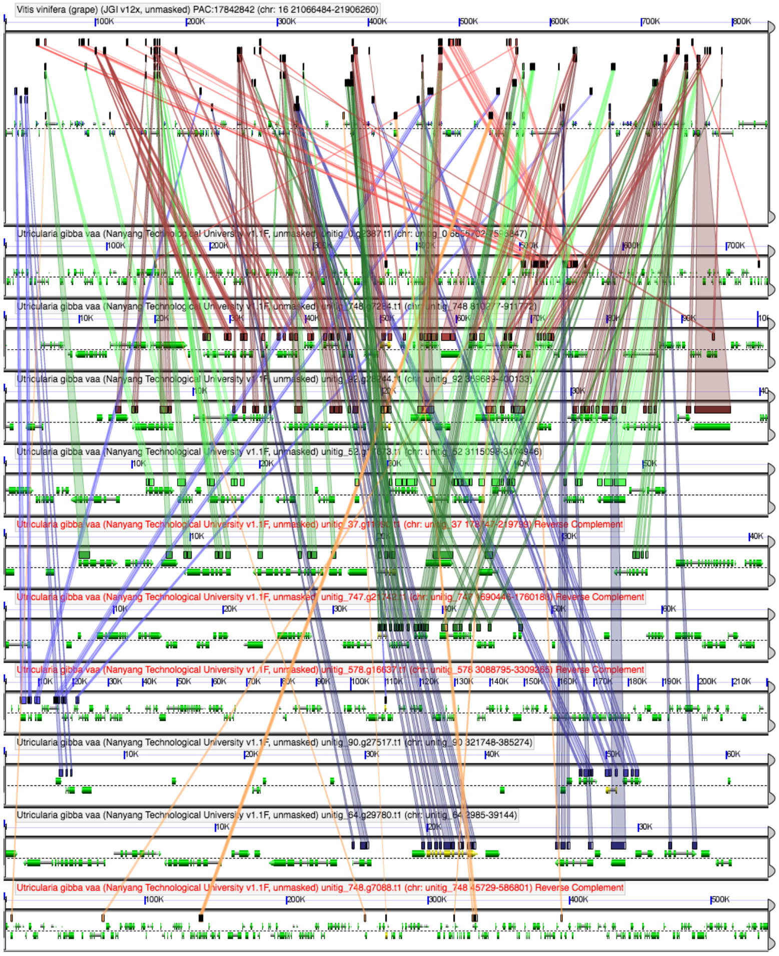

Fig. S22. GEvo plot for *Vitis* chr16. CoGe website link: https://genomevolution.org/coge//GEvo.pl?prog=blastz;iw=1000;fh=10;padding=1;hsp_top=1;nt=0;cbc=0;spike_len=15;ca=1;skip_feat_overlap=1;skip_hsp_overlap=1;hs=0;bzW=8;bzK=3000;bzO=400;bzE=30;accn1=PAC%3A17842842;fid1=391309733;dsid1=80882;dsgid1=19990;chr1=16;dr1up=381041;dr1down=455942;ref1=1;mask1=non-cds;accn2=unitig_0.g2387.t1;fid2=826717414;dsid2=98983;dsgid2=28800;chr2=unitig_0;dr2up=370000;dr2down=370000;ref2=0;mask2=non-cds;accn3=unitig_748.g7284.t1;fid3=826761164;dsid3=98983;dsgid3=28800;chr3=unitig_748;dr3up=50000;dr3down=50000;ref3=0;mask3=non-cds;accn4=unitig_92.g28244.t1;fid4=826775990;dsid4=98983;dsgid4=28800;chr4=unitig_92;dr4up=20000;dr4down=20000;ref4=0;mask4=non-cds;accn5=unitig_52.g17673.t1;fid5=826744210;dsid5=98983;dsgid5=28800;chr5=unitig_52;dr5up=-54522;dr5down=110000;ref5=0;mask5=non-cds;accn6=unitig_37.g11990.t1;fid6=826736442;dsid6=98983;dsgid6=28800;chr6=unitig_37;dr6up=20000;dr6down=20000;rev6=1;ref6=0;mask6=non-cds;accn7=unitig_747.g21742.t1;fid7=826759988;dsid7=98983;dsgid7=28800;chr7=unitig_747;dr7up=34147;dr7down=34737;rev7=1;ref7=0;mask7=non-cds;accn8=unitig_578.g16637.t1;fid8=826747360;dsid8=98983;dsgid8=28800;chr8=unitig_578;dr8up=110000;dr8down=110000;rev8=1;ref8=0;mask8=non-cds;accn9=unitig_90.g27517.t1;fid9=826775418;dsid9=98983;dsgid9=28800;chr9=unitig_90;dr9up=50000;dr9down=12610;ref9=0;mask9=non-cds;accn10=unitig_64.g29780.t1;fid10=826751472;dsid10=98983;dsgid10=28800;chr10=unitig_64;dr10up=20000;dr10down=20000;ref10=0;mask10=non-cds;accn11=unitig_748.g7088.t1;fid11=826760818;dsid11=98983;dsgid11=28800;chr11=unitig_748;dr11up=270000;dr11down=270000;rev11=1;ref11=0;mask11=non-cds;num_seqs=11;hsp_overlap_limit=0;hsp_size_limit=0

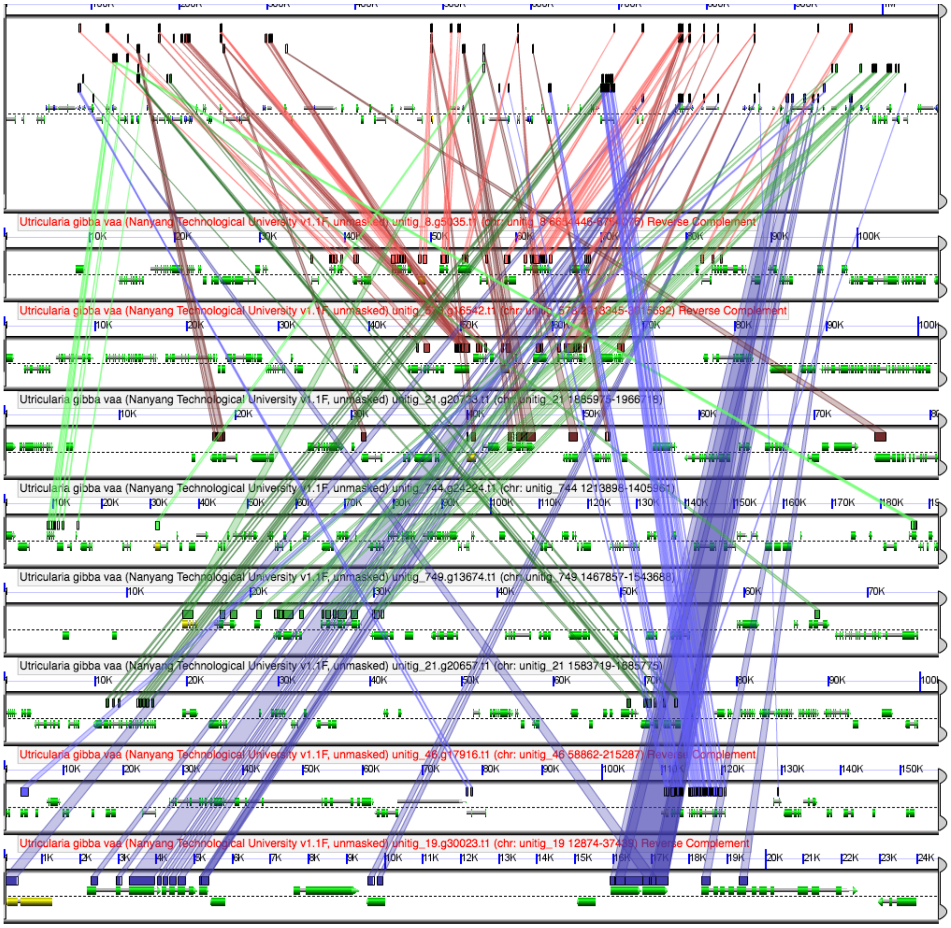
Utricularia gibba vaa (Nanyang Technological University v1.1F, unmasked) unitig_8.g5035.t1 (chr: unitig_8 6654446-6754076) Reverse Complement
Utricularia gibba vaa (Nanyang Technological University v1.1F, unmasked) unitig_578.g16542.t1 (chr: unitig_578 2913345-3015692) Reverse Complement
Utricularia gibba vaa (Nanyang Technological University v1.1F, unmasked) unitig_21.g20733.t1 (chr: unitig_21 1885975-1966718)
Utricularia gibba vaa (Nanyang Technological University v1.1F, unmasked) unitig_744.g24224.t1 (chr: unitig_744 1213898-1405961)
Utricularia gibba vaa (Nanyang Technological University v1.1F, unmasked) unitig_749.g13674.t1 (chr: unitig_749 1467857-1543688)
Utricularia gibba vaa (Nanyang Technological University v1.1F, unmasked) unitig_21.g20657.t1 (chr: unitig_21 1583719-1685775)
Utricularia gibba vaa (Nanyang Technological University v1.1F, unmasked) unitig_46.g17916.t1 (chr: unitig_46 58862-215287) Reverse Complement
Utricularia gibba vaa (Nanyang Technological University v1.1F, unmasked) unitig_19.g30023.t1 (chr: unitig_19 12874-37439) Reverse Complement

Fig. S23. GEvo plot for *Vitis* chr18. CoGe website link: https://genomevolution.org/coge//GEvo.pl?prog=blastz;iw=1000;fh=10;padding=1;hsp_top=1;nt=0;cbc=0;spike_len=15;ca=1;skip_feat_overlap=1;skip_hsp_overlap=1;hs=0;bzW=8;bzK=3000;bzO=400;bzE=30;accn1=PAC%3A17821841;fid1=391316180;dsid1=80882;dsgid1=19990;chr1=18;dr1up=486751;dr1down=576416;ref1=1;mask1=non-cds;accn2=unitig_8.g5035.t1;fid2=826770172;dsid2=98983;dsgid2=28800;chr2=unitig_8;dr2up=48676;dr2down=60088;rev2=1;ref2=0;mask2=non-cds;accn3=unitig_578.g16542.t1;fid3=826747186;dsid3=98983;dsgid3=28800;chr3=unitig_578;dr3up=54524;dr3down=46945;rev3=1;ref3=0;mask3=non-cds;accn4=unitig_21.g20733.t1;fid4=826723670;dsid4=98983;dsgid4=28800;chr4=unitig_21;dr4up=40000;dr4down=40000;ref4=0;mask4=non-cds;accn5=unitig_744.g24224.t1;fid5=826757082;dsid5=98983;dsgid5=28800;chr5=unitig_744;dr5up=30838;dr5down=160000;ref5=0;mask5=non-cds;accn6=unitig_749.g13674.t1;fid6=826764462;dsid6=98983;dsgid6=28800;chr6=unitig_749;dr6up=14553;dr6down=60000;ref6=0;mask6=non-cds;accn7=unitig_21.g20657.t1;fid7=826723530;dsid7=98983;dsgid7=28800;chr7=unitig_21;dr7up=130000;dr7down=-28989;ref7=0;mask7=non-cds;accn8=unitig_46.g17916.t1;fid8=826740322;dsid8=98983;dsgid8=28800;chr8=unitig_46;dr8up=110000;dr8down=45200;rev8=1;ref8=0;mask8=non-cds;accn9=unitig_19.g30023.t1;fid9=826722082;dsid9=98983;dsgid9=28800;chr9=unitig_19;dr9up=30000;dr9down=23295;rev9=1;ref9=0;mask9=non-cds;num_seqs=9;hsp_overlap_limit=0;hsp_size_limit=0

5. Gene Ontology Enrichment Analyses

We obtained the generic gene ontology (GO) term annotations for *Arabidopsis* genes from TAIR and functionally annotated the RepBase-filtered *U. gibba* gene models by assigning the GO terms from their associated *Arabidopsis* gene annotation (see section 2.4, above). We then carried out GO term enrichment analyses of subsets of foreground genes versus all annotatable genes in the *U. gibba* genome as background using Fisher's exact test in GOATOOLS (https://github.com/tanghaibao/goatools) to discover whether subsets of genes relate to specific biological functions or metabolic pathways. The *U. gibba* whole-genome background was custom-generated as the set of *U. gibba* genes annotatable against *Arabidopsis* genes at *E*-value cutoff of 1E-05, accepting the topmost hit as the match.

5.1. GO Enrichment Analysis of Syntenic Genes in *U. gibba* and *Arabidopsis*

To investigate GO enrichment among syntenic gene duplicates descending from *U. gibba* lineage-specific WGDs, a self-to-self SynMap was generated within CoGe using the QUOTA-ALIGN algorithm (73) with default parameters. Syntenic gene pairs was then downloaded from CoGe and used as the foreground subset in the GO enrichment analysis. As shown in Dataset S5, the topmost significantly enriched terms (Bonferroni-corrected *p*-values < 0.05) were mostly transcriptional regulatory functions. For comparison, the same pipeline was carried out on internally syntenic *Arabidopsis* genes descending from its own 2 lineage-specific WGDs, from which highly similar results were obtained (Dataset S6). The *Arabidopsis* background was all genes in the genome.

5.2. GO Enrichment Analysis of Tandem Duplicates in *U. gibba* and *Arabidopsis*

The blast_to_raw script in the QUOTA-ALIGN package (https://github.com/tanghaibao/quota-alignment), incorporated in CoGe's SynMap application, was used to filter out tandem duplicates before synteny plotting as in section 5.1. These genes calculated to be tandem duplicates in *U. gibba* were downloaded from a CoGe SynMap results link and used as a foreground subset for GO enrichment analyses. In contrast to functional enrichments of syntenic genes, the topmost significantly enriched terms for tandem duplicates were secondary metabolic functions, including specific functions that could be anticipated for a carnivorous plant (Dataset S7). Genes with significantly enriched GO terms assigned to them and their annotations are listed in Dataset S8. Although the specifically enriched terms were different for *Arabidopsis* tandem duplicates, they are also related mostly to secondary metabolic activities (Dataset S9). The *Arabidopsis* background used was all genes in its genome.

6. Molecular Evolution Analyses of Tandem Duplicated Genes

6.1. Cysteine Protease Genes

Cysteine protease genes identified within the collection of tandem duplicates derived in section 5.2 were used as queries for a NCBI local tblastx against *V. vinifera* (id 19990), *Arabidopsis* Col-0 (id 24424), *S. lycopersicum* (id 24769), and *U. gibba* (PacBio v1.1; id 28048) coding sequence databases downloaded from CoGe. The *Dionaea muscipula* cysteine protease (GenBank Accession KP663370) was also included in the dataset. Gene model repredictions were conducted using default settings of AUGUSTUS (21) with the genomic sequence of the previously predicted *U. gibba* gene models, plus 500-1000 bp of upstream and downstream genomic sequence. Two tandem duplicates (g1 and g2) were repredicted at locus utg699.g19345. Multiple sequence alignments were performed for CDS sequences using MAFFT E-INS-i (74). Regions corresponding to the variable signal peptide and propeptide were removed prior to phylogenetic analysis. Alignments were translated prior to phylogenetic analyses. Maximum-likelihood (ML) searches were used to reconstruct the cysteine protease phylogeny using RAxML v8.2.4 (75) on the CIPRES Science Gateway (http://www.phylo.org/index.php/) under the WAG+G model of evolution, as determined by the Akaike and Bayesian Information Criterion (AIC/BIC) in ProtTest v3.2 (76). Searches for the phylogenetic reconstruction with the highest likelihood score were performed simultaneously with rapid bootstrapping, allowing RAxML to automatically halt the analysis (at 552 bootstrap replicates). The resulting phylogeny was visualized using FigTree v1.4.0 (http://tree.bio.ed.ac.uk/software/figtree/). The multiple sequence alignment and the resulting phylogeny used for subsequent molecular evolutionary analyses are provided in Dataset S11.

We estimated ω (dN/dS) values for the cysteine protease CDS alignment and RAxML phylogeny using the codeml part of the PAML v4.4 package (77). Gaps in the alignment were excluded by PAML. Two types of models were implemented: "branch-specific" (ω ratio estimated for each branch in the tree (78)) and "branch-site" models (ω ratio varies in selected branches and across codons (79)).

Comparisons of two nested models were performed using a Likelihood Ratio Test (LRT) to test for the following: asymmetric sequence evolution (one-ratio model 0 ($\omega_0 = p_1$) versus two-ratio model 2 (ω_0, ω_1)), divergent selection (model 3 (discrete) versus clade model D ($K = 3$)), and positive selection (model A null ($\omega_2 = 1$) versus model A ($0 < \omega_0 < 1$). The chi square test was conducted using the log likelihood results of each branch and node of the phylogeny (Dataset S10; Cysteine Protease PAML Branches and Cysteine Protease PAML Nodes, Sheets 1 and 2). Sites listed as under positive selection in Dataset S10 correspond to amino acid residues in the multiple sequence alignment (Datasets S11-13) when gaps were removed by PAML. For subsequent homology modeling analyses of *U. gibba* cysteine protease, we matched sites identified by PAML as under positive selection in the un-gapped alignment to the original sites within contigs part of the alignment containing gaps (Datasets S10 and S11).

6.1.1. Cysteine Protease Homology Modeling

The protein structural model for the unitig699.g19348 catalytic domain was computed using the SWISS-MODEL server homology modeling pipeline (80) using PROMOD-II (81) and MODELLER (82). A crystal structure of a cysteine protease from *Dionaea muscipula* (PDB ID: 5a24) was identified as the top-ranking template in covalent complex with inhibitor E-64 (83). The program MacPyMOL v1.3 (Schrödinger LLC) was used to thread the 3D model of unitig_699.g19348 to 5a24 associated with E-64. Sites identified as evolving under positive selection pressure by the codeml branch-site model were mapped to PDB coordinates to detect substrate interacting regions and amino acids lining the substrate-binding cleft. Three (E24, V69, S160) of the unitig699.g19348 amino acid sites under positive selection (BEB confidence > 0.82, Bonferroni corrected $p < 0.0015$) are within five amino acids of the *D. muscipula* functional residues and line the substrate-binding cleft in the model (Dataset S10; Fig 3B and C in main text).

6.2. *KCS6*-like Genes

KCS6-like genes identified in the tandem duplicate analysis were used as a queries for NCBI local TBLASTX runs against *V. vinifera* (id 19990), *Arabidopsis* Col-0 (id 24424), *S. lycopersicum* (id 24769), and *U. gibba* (PacBio v1.1; id 28048) coding sequence databases downloaded from CoGe. Gene model reprediction was conducted as in section 6.1. Translated hits from the BLAST search were used to create an alignment in SeaView (84) using MUSCLE. Poorly aligned sequences were removed, the sequences were aligned again, and then the alignment was trimmed using Gblocks (85), with stringency parameters to allow smaller blocks, gap positions within the final blocks, and less strict flanking positions. Phylogenetic analysis was performed on back-translated nucleotide sequences using PhyML under default parameters in SeaView. As in section 6.1, ω values were estimated using the codeml program part of the PAML v4.4 package. The chi square test was conducted using the log-likelihood results of each branch and node of the phylogeny (Dataset S10; KCS PAML Branches and KCS PAML Nodes, Sheets 3 and 4). The multiple sequence alignment and resulting phylogeny for PAML analysis are available in Dataset S12.

6.3. *SVP*-like Genes

The *SVP*-like genes of *Arabidopsis*, tomato and grape were acquired from an ongoing MADS-box gene family analysis of 7 angiosperms being conducted by coauthors T.-H.C. and V.A.A. *U. gibba SVP*-like genes were identified by using the *Arabidopsis* and tomato SVP-like genes downloaded from TAIR (www.arabidopsis.org) to search against the *U. gibba* whole genome coding sequence dataset (PacBio v1.1; id 28048) by CoGeBlast with the TBLASTX algorithm with an *E*-value cutoff of 1E-10. Gene models were repredicted on the GeneWise website (86) for previously poorly predicted gene models. Genomic sequences of the target genes were acquired from CoGe and 5000 base pairs both upstream and downstream were added. Protein sequences serving as templates were selected based on the gene subfamily phylogeny. Default parameters were applied to the gene model reprediction with the modeled split site setting. All *SVP*-like genes from four species were aligned using MUSCLE, and non-informative regions were removed using Gblocks (85), with stringency parameters to allow smaller blocks, gap positions within the final blocks, and less strict flanking positions. The phylogenetic analysis was performed on back-translated nucleotide sequences using PhyML under default parameters in SeaView (84). As in 6.1**,** ω values were estimated using the codeml part of the PAML v4.4 package. The chi square test was conducted using the log-likelihood results of each branch and node of the phylogeny (Dataset S10; SVP PAML Branches and SVP PAML Nodes, Sheets 5 and 6). The multiple sequence alignment and resulting phylogeny for PAML analysis are available in Dataset S13.

References

1. Peterson D, Boehm K, & Stack S (1997) Isolation of milligram quantities of nuclear DNA from tomato (*Lycopersicon esculentum*), A plant containing high levels of polyphenolic compounds. *Plant Mol. Biol. Rep.* 15(2):148-153.
2. Ibarra-Laclette E*, et al.* (2013) Architecture and evolution of a minute plant genome. *Nature* 498(7452):94-98.
3. Long Q*, et al.* (2013) Massive genomic variation and strong selection in Arabidopsis thaliana lines from Sweden. *Nature genetics* 45(8):884-890.
4. Chin CS*, et al.* (2013) Nonhybrid, finished microbial genome assemblies from long-read SMRT sequencing data. *Nat. Methods* 10(6):563-569.
5. Walker BJ*, et al.* (2014) Pilon: an integrated tool for comprehensive microbial variant detection and genome assembly improvement. *PLOS One* 9(11):e112963.
6. Camacho C*, et al.* (2009) BLAST+: architecture and applications. *BMC bioinformatics* 10:421.
7. Salter S*, et al.* (2014) Reagent contamination can critically impact sequence-based microbiome analyses. *BMC Biology*.
8. Gualberto JM*, et al.* (2014) The plant mitochondrial genome: dynamics and maintenance. *Biochimie* 100:107-120.
9. Mao M, Austin AD, Johnson NF, & Dowton M (2013) Coexistence of minicircular and a highly rearranged mtDNA molecule suggests that recombination shapes mitochondrial genome organization. *Mol. Biol. Evol.*
10. VanBuren R*, et al.* (2015) Single-molecule sequencing of the desiccation-tolerant grass *Oropetium thomaeum*. *Nature*.
11. Quesneville H*, et al.* (2005) Combined evidence annotation of transposable elements in genome sequences. *PLoS computational biology* 1(2):166-175.
12. Flutre T, Duprat E, Feuillet C, & Quesneville H (2011) Considering transposable element diversification in *de novo* annotation approaches. *PloS One* 6(1).
13. Kohany O, Gentles AJ, Hankus L, & Jurka J (2006) Annotation, submission and screening of repetitive elements in Repbase: RepbaseSubmitter and Censor. *BMC bioinformatics* 7:474.
14. Wicker T*, et al.* (2007) A unified classification system for eukaryotic transposable elements. *Nature reviews. Genetics* 8(12):973-982.
15. Lagesen K*, et al.* (2007) RNAmmer: consistent and rapid annotation of ribosomal RNA genes. *Nucleic Acids Res.* 35(9):3100-3108.
16. Lowe T & Eddy S (1997) tRNAscan-SE: a program for improved detection of transfer RNA genes in genomic sequence. *Nucleic Acids Res.* 25(5):955-964.
17. Nawrocki E & Eddy S (2013) Infernal 1.1: 100-fold faster RNA homology searches. *Bioinformatics* 29(22):2933-2935.
18. Gardner PP*, et al.* (2011) Rfam: Wikipedia, clans and the "decimal" release. *Nucleic Acids Res.* 39(Database issue):D141-145.
19. Burge SW*, et al.* (2013) Rfam 11.0: 10 years of RNA families. *Nucleic Acids Res.* 41(Database issue):D226-232.

20. Stanke M, Diekhans M, Baertsch R, & Haussler D (2008) Using native and syntenically mapped cDNA alignments to improve *de novo* gene finding. *Bioinformatics* 24(5):637-644.
21. Hoff KJ & Stanke M (2013) WebAUGUSTUS-a web service for training AUGUSTUS and predicting genes in eukaryotes. *Nucleic Acids Res.* 41(W1):W123-W128.
22. Ibarra-Laclette E*, et al.* (2011) Transcriptomics and molecular evolutionary rate analysis of the bladderwort (*Utricularia*), a carnivorous plant with a minimal genome. *BMC Plant Biol.* 11(1):101.
23. Campbell MS, Holt C, Moore B, & Yandell M (2014) Genome annotation and curation using MAKER and MAKER‐P. *Curr. Protoc. Bioinformatics*:4.11.11-14.11.39.
24. Jurka J*, et al.* (2005) Repbase Update, a database of eukaryotic repetitive elements. *Cytogenetic and genome research* 110(1-4):462-467.
25. Kalendar R*, et al.* (2004) Large retrotransposon derivatives: abundant, conserved but nonautonomous retroelements of barley and related genomes. *Genetics* 166(3):1437-1450.
26. Thorvaldsdottir H, Robinson JT, & Mesirov JP (2013) Integrative Genomics Viewer (IGV): high-performance genomics data visualization and exploration. *Brief Bioinform.* 14.
27. Ibarra-Laclette E*, et al.* (2011) Transcriptomics and molecular evolutionary rate analysis of the bladderwort (*Utricularia*), a carnivorous plant with a minimal genome. *BMC Plant Biol.* 11(1):101.
28. Liao Y, Smyth GK, & Shi W (2013) The Subread aligner: fast, accurate and scalable read mapping by seed-and-vote. *Nucleic Acids Res.* 41(10):e108-e108.
29. Liao Y, Smyth GK, & Shi W (2013) featureCounts: an efficient general purpose program for assigning sequence reads to genomic features. *Bioinformatics*:btt656.
30. Robinson MD, McCarthy DJ, & Smyth GK (2010) edgeR: a Bioconductor package for differential expression analysis of digital gene expression data. *Bioinformatics* 26(1):139-140.
31. Benson G (1999) Tandem repeats finder: a program to analyze DNA sequences. *Nucleic Acids Res.* 27(2):573-580.
32. Edgar RC (2010) Search and clustering orders of magnitude faster than BLAST. *Bioinformatics* 26(19):2460-2461.
33. Fulnečková J*, et al.* (2013) A broad phylogenetic survey unveils the diversity and evolution of telomeres in eukaryotes. *Genome Biol. Evol.* 5(3):468-483.
34. Tran TD*, et al.* (2015) Centromere and telomere sequence alterations reflect the rapid genome evolution within the carnivorous plant genus *Genlisea*. *Plant J.* 84(6):1087-1099.
35. Bennetzen JL & Wang H (2014) The contributions of transposable elements to the structure, function, and evolution of plant genomes. *Ann. Rev. Plant* 65(1):505-530.
36. Melters DP*, et al.* (2013) Comparative analysis of tandem repeats from hundreds of species reveals unique insights into centromere evolution. *Genome biology* 14(1):R10.
37. Alkan C, Sajjadian S, & Eichler EE (2011) Limitations of next-generation genome sequence assembly. *Nat. Methods* 8(1):61-65.
38. McCoy RC*, et al.* (2014) Illumina TruSeq synthetic long-reads empower *de novo* assembly and resolve complex, highly-repetitive transposable elements. *PLoS One* 9(9):e106689.
39. Hayden KE & Willard HF (2012) Composition and organization of active centromere sequences in complex genomes. *BMC Genomics* 13(1):1-13.
40. Lyons E*, et al.* (2008) Finding and comparing syntenic regions among *Arabidopsis* and the outgroups papaya, poplar and grape: CoGe with rosids. *Plant Physiol.* 148:1772-1781.
41. Freeling M, Xu J, Woodhouse M, & Lisch D (2015) A solution to the C-value paradox and the function of junk DNA: the genome balance hypothesis. *Mol. Plant* 8(6):899-910.
42. Kurtz S*, et al.* (2004) Versatile and open software for comparing large genomes. *Genome biology* 5(2):R12.
43. Krzywinski M*, et al.* (2009) Circos: an information aesthetic for comparative genomics. *Genome Res.* 19.

44. Meraldi P, McAinsh AD, Rheinbay E, & Sorger PK (2006) Phylogenetic and structural analysis of centromeric DNA and kinetochore proteins. *Genome biology* 7(3):R23.
45. Birchler JA, Gao Z, & Han F (2009) A tale of two centromeres--diversity of structure but conservation of function in plants and animals. *Functional & integrative genomics* 9(1):7-13.
46. Wang G, Zhang X, & Jin W (2009) An overview of plant centromeres. *Journal of genetics and genomics = Yi chuan xue bao* 36(9):529-537.
47. Wade CM*, et al.* (2009) Genome sequence, comparative analysis, and population genetics of the domestic horse. *Science* 326(5954):865-867.
48. Nasuda S, Hudakova S, Schubert I, Houben A, & Endo TR (2005) Stable barley chromosomes without centromeric repeats. *Proceedings of the National Academy of Sciences of the United States of America* 102(28):9842-9847.
49. Locke DP*, et al.* (2011) Comparative and demographic analysis of orang-utan genomes. *Nature* 469(7331):529-533.
50. Liu Z*, et al.* (2008) Structure and dynamics of retrotransposons at wheat centromeres and pericentromeres. *Chromosoma* 117(5):445-456.
51. Cheng Z*, et al.* (2002) Functional rice centromeres are marked by a satellite repeat and a centromere-specific retrotransposon. *Plant Cell* 14.
52. Nagaki K*, et al.* (2005) Structure, divergence, and distribution of the CRR centromeric retrotransposon family in rice. *Molecular Biol. Evol.* 22(4):845-855.
53. Zhong CX*, et al.* (2002) Centromeric retroelements and satellites interact with maize kinetochore protein CENH3. *Plant Cell* 14(11):2825-2836.
54. Hudakova S*, et al.* (2001) Sequence organization of barley centromeres. *Nucleic Acids Res.* 29(24):5029-5035.
55. Gorin≈°ek B, Guben≈°ek F, & Kordi≈° Da (2004) Evolutionary genomics of chromoviruses in eukaryotes. *Mol. Biol. Evol.* 21(5):781-798.
56. Neumann P*, et al.* (2011) Plant centromeric retrotransposons: a structural and cytogenetic perspective. *Mobile DNA* 2(1):1.
57. Gorinsek B, Gubensek F, & Kordis D (2005) Phylogenomic analysis of chromoviruses. *Cytogenet Genome Res.* 110.
58. Gorinšek B, Gubenšek F, & Kordiš D (2004) Evolutionary genomics of chromoviruses in eukaryotes. *Mol. Biol. Evol.* 21(5):781-798.
59. Xu Z & Wang H (2007) LTR_FINDER: an efficient tool for the prediction of full-length LTR retrotransposons. *Nucleic Acids Res.* 35(suppl 2):W265-W268.
60. Edgar RC (2004) MUSCLE: multiple sequence alignment with high accuracy and high throughput. *Nucleic Acids Res.* 32.
61. Miller MA, Pfeiffer W, & Schwartz T (2010) Creating the CIPRES Science Gateway for inference of large phylogenetic trees. *Gateway Computing Environments Workshop (GCE), 2010*, (IEEE), pp 1-8.
62. Slotkin RK & Martienssen R (2007) Transposable elements and the epigenetic regulation of the genome. *Nat. Rev. Genet.* 8(4):272-285.
63. Topp CN, Zhong CX, & Dawe RK (2004) Centromere-encoded RNAs are integral components of the maize kinetochore. *Pro. Natl. Acad. Sci. USA* 101(45):15986-15991.
64. Gao X, Hou Y, Ebina H, Levin HL, & Voytas DF (2008) Chromodomains direct integration of retrotransposons to heterochromatin. *Genome Res.* 18.
65. Vanneste K, Van de Peer Y, & Maere S (2013) Inference of genome duplications from age distributions revisited. *Molecular biology and evolution* 30(1):177-190.
66. Makova KD & Hardison RC (2015) The effects of chromatin organization on variation in mutation rates in the genome. *Nature Rev. Genet.* 16(4):213-223.
67. Lyons E & M F (2008) How to usefully compare homologous plant genes and chromosomes as DNA sequences. *Plant J.* 53(4):661-673.

68. Librado P & Rozas J (2013) Uncovering the functional constraints underlying the genomic organization of the odorant-binding protein genes. *Genome Biol. Evol.* 5:2096-2108.
69. Li H*, et al.* (2009) The sequence alignment/map format and SAMtools. *Bioinformatics* 25(16):2078-2079.
70. McKenna A*, et al.* (2010) The Genome Analysis Toolkit: a MapReduce framework for analyzing next-generation DNA sequencing data. *Genome Res.* 20(9):1297-1303.
71. Tang H*, et al.* (2008) Synteny and collinearity in plant genomes. *Science* 320(5875):486-488.
72. Tang H*, et al.* (2015) SynFind: Compiling Syntenic Regions across Any Set of Genomes on Demand. *Genome Biol. Evol.* 7(12):3286-3298.
73. Tang H*, et al.* (2011) Screening synteny blocks in pairwise genome comparisons through integer programming. *BMC bioinformatics* 12(1):1.
74. Katoh K & Standley DM (2013) MAFFT multiple sequence alignment software version 7: improvements in performance and usability. *Mol. Biol. Evol.* 30(4):772-780.
75. Stamatakis A (2014) RAxML version 8: a tool for phylogenetic analysis and post-analysis of large phylogenies. *Bioinformatics* 30(9):1312-1313.
76. Abascal F, Zardoya R, & Posada D (2005) ProtTest: Selection of best-fit models of protein evolution. *Bioinformatics* 21:2104-2105.
77. Yang Z (2007) PAML 4: phylogenetic analysis by maximum likelihood. *Mol. Biol. Evol.* 24(8):1586-1591.
78. Yang Z (1998) Likelihood ratio tests for detecting positive selection and application to primate lysozyme evolution. *Mol. Biol. Evol.* 15(5):568-573.
79. Yang Z & Nielsen R (2002) Codon-substitution models for detecting molecular adaptation at individual sites along specific lineages. *Mol. Biol. Evol.* 19(6):908-917.
80. Biasini M*, et al.* (2014) SWISS-MODEL: modelling protein tertiary and quaternary structure using evolutionary information. *Nucleic Acids Res.* 42(W1):W252-W258.
81. Guex N & Peitsch MC (1997) SWISS-MODEL and the Swiss-PdbViewer: an environment for comparative protein modeling. *Electrophoresis* 18(15):2714-2723.
82. Sali A & Blundell TL (1993) Comparative protein modelling by satisfaction of spatial restraints. *J. Mol. Biol.* 234(3):779-815.
83. Risør MW*, et al.* (2015) Enzymatic and structural characterization of the major endopeptidase in the Venus flytrap digestion fluid. *J. Biol. Chem.*:jbc.M115.672550.
84. Gouy M, Guindon S, & Gascuel O (2010) SeaView version 4: a multiplatform graphical user interface for sequence alignment and phylogenetic tree building. *Molecular biology and evolution* 27(2):221-224.
85. Talavera G & Castresana J (2007) Improvement of phylogenies after removing divergent and ambiguously aligned blocks from protein sequence alignments. *Syst. Biol.* 56(4):564-577.
86. Birney E, Clamp M, & Durbin R (2004) GeneWise and genomewise. *Genome Res.* 14(5):988-995.